Tree Genetics & Genomes (2017) 13:112
DOI 10.1007/s11295-017-1194-0

ORIGINAL ARTICLE

3D phenotyping and QTL analysis of a complex character: rose bush architecture

Camille Li-Marchetti[1] · Camille Le Bras[2] · Annie Chastellier[2] · Daniel Relion[2] · Philippe Morel[2] · Soulaiman Sakr[2] · Laurence Hibrand-Saint Oyant[2] · Laurent Crespel[2]

Received: 25 April 2017 / Revised: 11 September 2017 / Accepted: 12 September 2017

Abstract Plant shape, and thereby plant architecture, is a major component of the visual quality of ornamental plants. We have been developing a new method for analyzing the entire plant architecture by 3D digitalization that allows an almost exhaustive description of rose bush architecture and generates a large number of variables, many of them inaccessible manually. We carried out a QTL analysis using this original phenotyping method. In order to evaluate a broader allelic variability as well as the effect of the genetic background on QTL detection, we used two connected, segregating, recurrent blooming populations. The number of QTLs per variable varied from three for the number of determined axes (NbDetA) to seven for the branching angle of order 2 long axes (AngLA2), the two populations taken together. Five new QTLs, located on the linkage groups (LGs) 2, 6, and 7, were detected for the branching angle of axes, and the QTL located on LG7 co-localized with *RhBRC1*, a branching repressor. Branching and stem elongation QTLs also co-located with *RhBRC1*, suggesting its pleiotropic nature. Year-specific QTLs were also revealed, that explained the genotype × year interactions observed for the number of order 3 short axes (NbSA3) and AngLA2 from a genetic point of view. We also evidenced an effect of the genetic background on QTL detection. This new knowledge should help to better reason the genetic improvement programs for rose bush architecture and, therefore, rose bush shape.

Keywords Shape · 3D digitalization · Connected populations · *BRC1* · Year-specific QTL · Genetic background effect

Introduction

Overall plant shape is a major component of the visual quality of potted ornamental plants (Boumaza et al. 2009). It results from the architectural construction of the plant, i.e., the positioning of the different aerial organs in space according to organization rules that are specific to each species. Plant architecture is the result of growth and branching processes that depend on genetic and environmental factors and their interactions, as shown in rose bush (Crespel et al. 2014; Li-Marchetti et al. 2015).

Plant shape can therefore be controlled genetically (by plant breeding) and/or environmentally, including cultivation techniques such as water restriction (Demotes-Mainard et al. 2013; Li-Marchetti et al. 2015), modification of the light spectrum (Demotes-Mainard et al. 2016; Huché-Thélier et al. 2016), and mechanical stimulation (Morel et al. 2012). These factors make it possible to modify architectural characteristics such as metamer length or the number and the position of branches along the axis. However, these methods are applied more or less empirically by plant breeders and

Laurence Hibrand-Saint Oyant and Laurent Crespel contributed equally to this work.

Communicated by D. Chagné

Electronic supplementary material The online version of this article (https://doi.org/10.1007/s11295-017-1194-0) contains supplementary material, which is available to authorized users.

✉ Laurent Crespel
laurent.crespel@agrocampus-ouest.fr

[1] ASTREDHOR – Institut Technique de l'Horticulture, Paris, France

[2] IRHS, INRA, AGROCAMPUS OUEST, Université d'Angers, SFR 4207 QUASAV, 42 rue Georges Morel, 49071 Beaucouzé cedex, France

Published online: 30 September 2017

horticulturists. More extensive knowledge about the heredity of architectural characteristics as well as the genotype × environment interaction could lead to a more effective control of the plant architecture and thereby its shape.

We selected rose bush as a model plant for its economic value (Debener and Linde 2009), but also because it displays strong variability in shape and therefore in architecture too, ranging from a spreading to an upright growth habit (Gudin 2000).

Plant architecture is a complex character when it comes to phenotyping. Until now, the analysis of its heredity in rose bush had been limited to some architectural characteristics easily measurable manually such as the diameter, the number of internodes and stem length (Yan et al. 2007), and the architectural characteristics of the flowering axis (Kawamura et al. 2011, 2015). Taking into account the entire plant architecture would make it possible to analyze new variables, and more particularly, focus on the most relevant ones, i.e., those that are most explanatory of the variability observed in rose bush and least correlated.

To meet this objective, an analysis method of the entire architecture of rose bush by 3D digitalization was developed over the last years (Morel et al. 2009; Crespel et al. 2013). It consists in breaking down the plant into axes and metamers (internodes), which are in turn characterized (i) morphologically, for example based on their length and their diameter; (ii) topologically, by determining how they are connected (succession or branching); and (iii) geometrically, by characterizing their organization in space, for example by studying the branching angle of the axis (Godin et al. 1999). The method yields an almost exhaustive description of the plant architecture and generates a large number of variables, many of them inaccessible manually. It was first applied to two rose bush cultivars with contrasting shapes and clearly distinguished their architecture based on a large number of variables (Morel et al. 2009). Then, it was applied to eight cultivars with contrasting shapes (ranging from upright to spreading) to select a limited number of variables necessary and sufficient to distinguish between different architectures. Six quantitative variables at the plant and axis scales were thus selected (Crespel et al. 2013).

In all previous studies, the genetic analysis of rose bush architecture was carried out by mapping, using a population that also segregated for the mode of flowering (Yan et al. 2007; Kawamura et al. 2011, 2015). It was made up of nonrecurrent blooming roses, which flower only once a year in spring, and recurrent blooming roses with continuous flowering. Significant architectural differences were observed between nonrecurrent and recurrent roses, highlighting a correlation between the mode of flowering and the plant architecture (Kawamura et al. 2015). The growth habit of nonrecurrent blooming roses was spreading, while it was upright for recurrent blooming roses. A major quantitative trait locus (QTL, $R^2 > 20\%$) was detected for plant shape near *RoKSN*, a homolog of *TERMINAL FLOWER 1* (*TFL1*) which controls the mode of flowering in rose bush (Kawamura et al. 2015; Iwata et al. 2012). Taking these observations into account, the genetic analysis of a population with a unique mode of flowering should help to detect QTLs that are specific to rose bush architecture.

Totals of 11, 28, and 16 QTLs were detected by Yan et al. (2007) in a diploid population originating from a cross between *Rosa multiflora*-derived genotypes and Kawamura et al. (2011, 2015) in a diploid population originating from a cross between 'The Fairy' and a hybrid of *Rosa wichurana*, respectively. One to six QTLs were involved in the control of the architectural characteristics (Yan et al. 2007; Kawamura et al. 2011, 2015). For stem diameter, an architectural characteristic in common between the two studies, the number of QTLs varied according to the study, with four QTLs detected by Yan et al. (2007) and two by Kawamura et al. (2015); it was probably population-dependent (i.e., genetic background-dependent). This effect of the genetic background had been observed in corn (Beavis et al. 1991; Li et al. 2007, 2009). To better characterize the QTLs involved in the control of a given character, several populations with various genetic backgrounds have to be considered. In accordance with this, the use of connected populations has been developed these last years for the genetic analysis of quantitative characters such as grain yield in corn (Blanc et al. 2006; Li et al. 2009) or bud phenology and fruit firmness in apple tree (Celton et al. 2011; Bink et al. 2014; Allard et al. 2016). Besides being well adapted to evaluate the effect of the genetic background on QTL detection, they make it possible to study a broader allelic variability.

Thus, the work initiated by Yan et al. (2007) and Kawamura et al. (2011, 2015) on the genetic analysis of rose bush architecture could be supplemented (i) by using the phenotyping method developed by Morel et al. (2009) and Crespel et al. (2013), which takes into account the entire plant architecture; (ii) by overcoming the effect of the mode of flowering on the plant architecture, using segregating, recurrent blooming populations; and (iii) by evaluating a broader allelic variability as well as the effect of the genetic background on QTL detection from connected populations.

The present study was designed to achieve this objective and therefore aimed to (i) phenotype by 3D digitalization the architecture of two segregating, recurrent blooming rose bush populations connected by their female parent 'The Fairy'; (ii) identify and select the most relevant variables to describe rose bush architecture and its variations, both in terms of plant and axis scales; (iii) estimate the broad sense heritability of the most relevant architectural variables; (iv) identify QTLs involved in the control of these variables; and (v) evaluate the effect of the genetic background on the detection of QTLs.

Materials and methods

Plant material

Two diploid ($2n = 2x = 14$), connected, recurrent blooming rose bush populations consisting of 132 and 157 individuals derived from crosses between 'The Fairy' × 'Old Blush' and 'The Fairy' × 'Perle d'Or' were used for QTL analyses. 'The Fairy' and 'Perle d'Or' are rose hybrids, whereas 'Old Blush' belongs to the *Rosa chinensis* species. The female parent 'The Fairy' is a commercial cultivar obtained from the cross 'Paul Crampel' × 'Lady Gay' in 1932 by Ann Bentall. The male parent 'Old Blush' was discovered by Parsons in 1793, and the male parent 'Perle d'Or' was obtained from the cross Polyantha × 'Madame Falcot' in 1875 by Joseph Rambaux. The parents are all diploid and recurrent blooming, with contrasting architectures (Crespel et al. 2013). 'The Fairy' has a large number of axes and branching orders and long axes with many metamers. In contrast, 'Perle d'Or' is characterized by a low number of axes and branching orders and long axes with few metamers, whereas 'Old Blush' has an intermediate number of axes, a high number of branching orders, and long axes with an intermediate number of metamers.

Experimental conditions

The study was carried out in the experimental facilities of the IRHS (French Research Institute on Horticulture and Seeds) in Angers. The experimental conditions described below were repeated twice: in the springtime in 2014 and 2015. For each studied year, plants were obtained from cuttings of 1-year-old plants grown in pots in the greenhouse. Cuttings were made of a single metamer—a unit composed of one internode, one node, its axillary bud, and one leaf (White 1979)—from the median zones of the stems. Cuttings were taken in January and planted into plugs (35 mm diameter, 40 mm height) composed of a nonwoven fabric containing a mixture of fine peat and perlite. They were placed under a plastic tunnel in a greenhouse for rooting. Average temperatures were 18 °C at night and 22 °C during the day, and relative humidity was maintained at saturation by a fine mist humidifier. After 5 weeks, the plants were planted in 0.5-L pots and then in 2-L pots 1 month later. The experiment was conducted in a greenhouse on 4.5 m^2 benches equipped with a nutrient solution tank. The soil water potential was measured by a tensiometer, and subirrigation was triggered when a threshold of − 10 kPa was reached. Mineral nutrition was provided by fertilization with a liquid fertilizer ($N\text{-}P_2O_5\text{-}K_2O$, 3:2:6, pH = 6.5, electroconductivity = 1.2 mS cm^{-1}). Minimum air temperature was maintained at 18 °C, with aeration at 20 °C. Relative humidity was maintained at 70%. No supplementary lighting was applied.

Regarding the rose bush architecture, nongenetic variance is mainly due to intraplant variance rather than variance among plants (Kawamura et al. 2011). The number of axes must therefore be given priority rather than the number of plants per individual. Moreover, for a limited number of plants (for reasons of experimental costs), it is better to increase the number of individuals of the progeny rather than the number of plants per individual for QTL detection (Knapp and Bridges 1990; De Vienne and Causse 1998). Therefore, the number of plants per individual was reduced to one for the benefit of the number of individuals, as recently applied by Pauly et al. (2012) in ray grass.

The average daily air temperature (in °C day) was measured to calculate the sum of temperatures according to the method used by Huché-Thélier et al. (2011) to define the time taken for the plants to develop in relation to a base temperature of 1.93 °C. Similarly, global solar radiation outside the greenhouse (Météo France, Beaucouzé, France) was recorded daily to calculate total radiation over the growing period (in J/cm^2; Table 1).

Collection of architectural data

The architectural analysis was carried out at the plant and axis scales (Crespel et al. 2013). At the plant scale, the variables included the number of determined axes, differentiating between short (one to four metamers) and long (five metamers or more) axes, as defined by Morel et al. (2009). At the axis scale, three categories of variables were measured, morphological (length…), topological (branching order…), and

Table 1 Climatic characterization of both years (2014 and 2015)

Month	Thermal time (°C day)		Difference[a] (%)	Cumulative irradiance (J/cm^2)		Difference (%)
	2014	2015		2014	2015	
March	385.0	411.6	+ 7.0	34.674	25.505	− 26.4
April	531.2	561.0	+ 5.6	48.090	50.623	+ 5.3
May	563.5	573.0	+ 1.7	60.150	58.772	− 2.3
June	621.5	666.5	+ 7.2	70.871	70.614	− 0.4
Total	2101.2	2212.1	+ 5.3	213.785	205.514	− 3.9

[a] Difference between the 2 years compared to 2014

geometric (branching angle…), for the two types of axes (Table 2).

These architectural measurements were performed at the elementary architectural structure (EAS) stage when the plants were approximately 5 months old with completely developed and branch-bearing axes of order 1, leading to a structure with axes that reached the flowering stage in several weeks (Crespel et al. 2013). Three long order 2 axes were selected per plant (Fig. 1). Architectural measurements were made on them and their branching from June 9th to July 9th in 2014 and from June 4th to June 25th in 2015. Plants that had reached the EAS stage were stored, not longer than 1 week, at 2 °C in a dark cold chamber to block their growth and branching (Girault et al. 2008; Djennane et al. 2013) and avoid any experimental bias. Each plant was defoliated before phenotyping. Architectural measurements were carried out using a Fastrack® digitizer (Polhemus, Colchester, VT, USA), and data were recorded using PiafDigit software (Donès et al. 2006) to store measurements and construct a 3D real-time representation of plant architecture. Data were coded in multiscale tree graph (MTG) format (Godin and Caraglio 1998). Variables were extracted from these data using AMAPmod software (Godin et al. 1999).

Analysis of architectural data

A total of 41 architectural variables were measured (Table 2). They were subjected to a principal component analysis (PCA), as described by Crespel et al. (2013). The first four principal components were selected. For each of them, the associated variables were classified according to their contribution to their formation, and for each of the abovementioned architectural categories, the best qualified one was selected.

The PCA was carried out on the average values of the 41 variables measured on the two connected populations in 2014 and 2015, using FactoMineR, an R package dedicated to multivariate data analysis.

Correlations between the set of selected variables were then calculated for each population and year (Pearson's correlation coefficient, $p < 0.05$), using Rcmdr package.

The normality of the distribution of residuals was checked for each variable using a quantile-quantile plot test. The residuals were extracted from the following linear model, using RVAideMemoire package: $P_{ijl} = \mu + G_i + Y_j + (G \times Y)_{ij} + e_{ijl}$, where P_{ij} is the phenotypic value of genotype i for the year j, μ is the overall mean of the progeny for all genotypes and years, G_i is the effect of the genotype i, Y_j is the effect of the year j, $(G \times Y)_{ij}$ is their interaction, and e_{ijl} is the residual error effect for the l measured axes per genotype.

When the distribution of residuals deviated from normality, neperian logarithm (ln) transformation was used to unskew distribution.

Analyses of variance, followed by multiple comparisons of means (Newman-Keuls test), were carried out on the variables, with a probability of $p < 0.05$, to reveal whether or not there was a significant effect of the factors genotype (G) and year (Y) and of the interaction between them. These statistical analyses were carried out using Rcmdr package.

Broad-sense heritability

The broad-sense heritability (H^2) of each variable was estimated as the ratio of the genotypic variance (σ^2_G) to the phenotypic variance (σ^2_P). The components of the phenotypic variance were calculated on the basis of the analysis of variance of the expected mean squares (ANOVA), as described by Nanson (1970) and used by Gitonga et al. (2014). The phenotypic variance was therefore calculated as follows:

$$\sigma^2_P = \sigma^2_G + \sigma^2_{GY} \Big/ Y + \sigma^2_\varepsilon \Big/ rY$$

where σ^2_{GY} is the variance of the $G \times Y$ interaction, σ^2_ε is the residual variance, Y is the number of years, and r is the number of replicates.

Collection of genotypic data

Genomic DNA from each individual from connected populations and parents was extracted from young leaves using NucleoSpin® 96 Plant II Kit (Macherey-Nagel, Düren, Germany), following the manufacturer's protocol, using the Zephir workstation of the ANAN platform (SFR QuaSaV, University of Angers, France).

A total of 79 molecular markers was used. Seventy-seven microsatellite markers (SSRs) belonging to several SSR sets (Online Resource 1) were used to construct the genetic maps: (i) genomic and EST-SSRs of rose (Hibrand-Saint Oyant et al. 2008), (ii) noncoding SSRs developed by the WIPO (World Intellectual Property Organization: http://patentscope.wipo.int/search/en/WO2003097869), (iii) genomic SSRs obtained by Meng et al. (2009), and (iv) SSRs from other *Rosaceae*, and two candidate genes on which our team works more particularly (Online Resource 2): *Branched 1*, a transcription factor known to be a branching repressor in rose (*RhBRC1*; Barbier et al. 2015), and *SUC2*, a sucrose/H+ co-transporter involved in the photocontrol of bud break in rose (*RhSUC2*; Henry et al. 2011).

SSR markers were analyzed as previously described by Kawamura et al. (2011) and Roman et al. (2015).

cDNA sequences of *RhBRC1* and *RhSUC2* were aligned with the *Fragaria vesca* genome. Based on this sequence alignment, specific PCR primers were designed to amplify a genomic sequence of 1 kbp.

PCR reactions were performed in a final volume of 20 μL containing 10 ng of genomic DNA, 0.2 mM of each dNTP, 0.5 μM of forward and reverse primers, 4 μL of 5× Phusion®

Table 2 List of the architectural variables measured, according to the four categories defined (plant description, axis morphology, topology, and geometry) and the contribution of these variables to the formation of principal components (PC) 1, 2, 3, and 4 of the principal component analysis

Variables	Code	Contribution of variables (%)			
		PC1	PC2	PC3	PC4
Plant scale					
Plant description					
Number of determined axes (axes terminated in a flower bud or a flower)	*NbDetA*	*8.1*	2.4	0.2	0.0
Number of order 3 determinated axes	NbDetA3	5.0	0.4	4.3	0.7
Number of order 4 determinated axes	NbDetA4	7.8	1.8	0.1	0.1
Number of order 5 determinated axes	NbDetA5	4.8	2.4	2.4	0.6
Number of metamers	NbMet	7.4	2.4	0.9	0.2
Number of long axes	NbLA	4.2	3.4	2.0	2.5
Number of order 3 long axes	NbLA3	3.3	1.1	0.3	4.1
Number of order 4 long axes	NbLA4	3.0	3.5	4.7	1.0
Number of short axes	NbSA	8.0	1.9	0.0	0.3
Number of order 3 short axes	*NbSA3*	2.7	0.0	*7.4*	0.6
Number of order 4 short axes	NbSA4	7.4	1.1	0.8	0.0
Number of order 5 short axes	NbSA5	4.8	2.3	2.1	0.7
Axis scale					
Axis morphology					
Number of metamers of the LAs	NbMetLA	0.1	2.1	3.1	8.7
Number of metamers of the order 2 LAs	NbMetLA2	2.9	0.3	6.3	0.0
Number of metamers of the order 3 LAs	NbMetLA3	0.9	0.0	0.6	2.6
Number of metamers of the order 4 LAs	NbMetLA4	0.0	0.1	0.4	8.2
Length of the LAs	*LLA*	0.3	5.7	0.1	*9.6*
Length of the order 2 LAs	LLA2	3.2	1.0	2.3	0.0
Length of the order 3 LAs	LLA3	1.4	1.7	3.7	6.6
Length of the order 4 LAs	LLA4	0.1	1.1	2.7	9.6
Number of metamers of the SAs	NbMetSA	0.4	0.7	5.2	0.3
Number of metamers of the order 3 SAs	NbMetSA3	0.8	0.0	1.4	0.0
Number of metamers of the order 4 SAs	NbMetSA4	0.0	0.0	9.8	0.0
Number of metamers of the order 5SAs	NbMetSA5	0.0	0.0	6.0	0.1
Length of the SAs	LSA	1.0	0.1	1.1	0.3
Length of the order 3 SAs	LSA3	0.6	0.6	1.1	1.3
Length of the order 4 SAs	*LSA4*	0.0	0.3	*10.6*	1.7
Length of the order 5 SAs	LSA5	0.0	0.2	5.8	1.5
Axis topology					
Number of branching orders	NbBrO	1.6	0.9	3.2	1.8
Number of branchings on the LAs	NbBrLA	3.0	0.1	4.3	6.3
Number of branchings on the LAs in the distal zone	*NbBrTopLA*	0.7	1.2	3.4	*12.2*
Number of branchings on the LAs in the median zone	NbBrMedLA	0.1	1.0	2.4	0.2
Number of branchings on the LAs in the basal zone	NbBrBasLA	2.1	0.3	0.0	1.2
Axis geometry					
Branching angle of the cord of the LAs in relation to the vertical axis	AngLA	2.5	8.8	0.1	2.3
Branching angle of the cord of the order 2 LAs in relation to the vertical axis	AngLA2	2.3	5.9	0.0	3.2
Branching angle of the cord of the order 3 LAs in relation to the vertical axis	AngLA3	2.2	8.4	0.0	2.2
Branching angle of the cord of the order 4 LAs in relation to the vertical axis	AngLA4	1.5	6.5	0.7	0.5

Table 2 (continued)

Variables	Code	Contribution of variables (%)			
		PC1	PC2	PC3	PC4
Branching angle of the cord of the SAs in relation to the vertical axis	*AngSA*	1.6	*9.5*	0.2	2.5
Branching angle of the cord of the order 3 SAs in relation to the vertical axis	AngSA3	2.0	6.8	0.1	3.5
Branching angle of the cord of the order 4 SAs in relation to the vertical axis	AngSA4	1.5	8.4	0.4	2.0
Branching angle of the cord of the order 5 SAs in relation to the vertical axis	AngSA5	0.7	5.4	0.2	0.6

In italics, selected variables

High-Fidelity buffer, and 0.4 U of Phusion® High-Fidelity DNA Polymerase (Thermo Fisher Scientific, Waltham, MA, USA). PCR amplification was performed with a MyCycler™ thermal cycler (Bio-Rad, Hercules, CA, USA), according to the following sequence: 30 s at 98 °C, 35 cycles of 30 s at 98 °C, annealing and extension steps of 30 s at 72 °C, and a final extension step of 10 min at 72 °C. For *RhBRC1*, 8 μL of PCR product was double-digested with *Pst*I and *Ase*I enzymes in a final volume of 25 μL, according to the manufacturer's recommendations (Thermo Fisher Scientific, Waltham, MA, USA). Electrophoretic separations of the digestion products were performed with a Labchip® GX (Caliper Life Sciences, Hopkinton, MA, USA) on the ANAN platform (SFR QuaSaV, University of Angers, France). For *RhSUC2*, PCR amplification products were separated by electrophoresis on 1.5% agarose gel, at a constant voltage of 100 V, for 25 min; DNA was stained with ethidium bromide.

Linkage analysis and map construction

Linkage analysis and map construction were performed with JoinMap® software version 4.1 (Van Ooijen 2011) using the cross-pollination (CP) model.

Parental maps were constructed separately using different sets of segregating markers: a set of markers present only in the female parent, a set present only in the male parent, and a set of biparental markers that showed heterozygosity in both parents.

Marker segregation distortion was tested against the expected Mendelian segregation ratio, using the chi-square test integrated in JoinMap® 4.1 software. Distorted markers were kept but were flagged (***$p < 0.01$; ****$p < 0.001$; *****$p < 0.0001$). The markers were classified into five different segregation classes depending on the allele patterns of the parents: (1) <lmxll>, (2) <nnxnp>, (3) <efxeg>, (4) <abxcd>, and (5) <hkxhk>. Parental configuration of the <abxcc> or <aaxbc> types with a segregation ratio of 1:1 is not supported by JoinMap® 4.1 software, so they were classified into classes 1 and 2, respectively.

Linkage groups (LGs) were estimated by applying an independence log-of-odds (LOD) threshold ranging from 3.0 to 10.0 with steps of 1.0. A LOD score of 5 was used to determine LGs. Maps were constructed using the Kosambi mapping function and the regression mapping algorithm up to round 2, with the following JoinMap parameters: Rec < 0.50; LOD > 1.0; Ripple = 1; Jump = 5; the jump

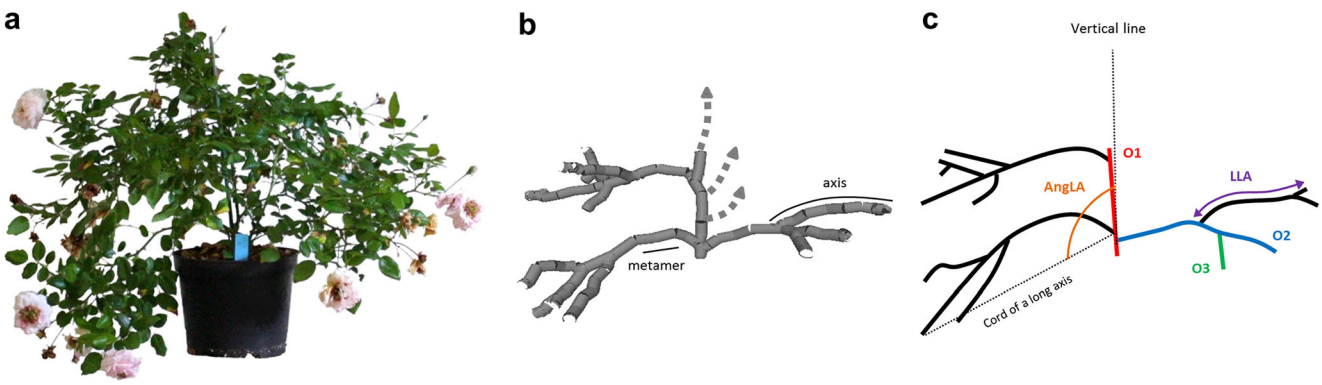

Fig. 1 Plant architectural traits phenotyping. Plant photography before phenotyping by 3D digitalization (**a**), plant architecture composed of three selected order 2 axes and their branches, with two components (metamer and axis), hatched bars represent the rest of plant (**b**), simplified representation with three branching orders: order 1 (O1), order 2 (O2), and order 3 (O3), the representation of the long axes length (LLA) and of the branching angle of the cord of the long axes in relation to the vertical axis (AngLA; **c**)

was occasionally set to 11.0 in case of conflicting markers that obstructed mapping.

Ungrouped or misplaced markers were reassigned based on the consensus map constructed by Spiller et al. (2011) and the strongest cross-link information, using the 'move to loci' function of the software. Markers with an undetermined linkage phase or insufficient linkage were removed. Maps were drawn using MapChart 2.2 software (Voorrips 2002).

QTL analysis

When the $G \times Y$ interaction was significant, a mixed linear model was built for the variable, as described by Celton et al. (2011) and Ben Sadok et al. (2013): $P_{ijl} = \mu + G_i + Y_j + (G \times Y)_{ij} + e_{ijl}$, where P_{ij} is the phenotypic value of genotype i for the year j, μ is the overall mean of the progeny for all genotypes and years, G_i is the random effect of the genotype i, Y_j is the fixed effect of the year j, $(G \times Y)_{ij}$ is their random interaction, and e_{ijl} is the residual error effect for the l measured axes per genotype.

The models were estimated using the residual maximum likelihood (REML) estimation method, and effects to be included were selected based on the Akaike information criterion (AIC). When G and $G \times Y$ effects were included, the best linear unbiased predictor (BLUP) was computed for the G and $G \times Y$ effects. The BLUPs for the $G \times Y$ effect were computed for each studied year. These statistical analyses were carried out using lme4, Car, and RVAideMemoire packages in R.

QTL detection was performed for each parental map directly on the transformed or untransformed data, on the G BLUP and the $G \times Y$ BLUP when available, using the R/qtl package.

Multiple QTL regression was carried out with the stepwiseqtl function, as described by Huang et al. (2012). This approach is based on forward/backward selection to compare a multiple QTL model with inclusion of both main effect QTLs and possible pairwise QTLxQTL interactions. The maximum number of QTLs was set to 10 for forward selection (max.qtl = 10). For each model, a penalized LOD score (pLOD; the log likelihood ratio comparing the full model to the null QTL-free model) was calculated, with penalties on the number of QTLs and pairwise QTLxQTL interactions. For each variable, these penalties were derived from 10,000 permutations with a 2D scan and a genome-wide error rate of 0.05. The QTL model with the largest pLOD was considered as the most probable one. Once the multiple QTL model was determined, QTL position ('refineqtl' function), the individual LOD score, and the estimated R^2 value for each term of the model and for the whole model were refined. The 'lodint' function was used to derive LOD-1 QTL location confidence intervals.

Results

Selecting the most relevant variables

Forty-one architectural variables were measured at the plant and axis scales and then submitted to a PCA. Components 1, 2, 3, and 4 of the PCA accounted for 23.7, 16.4, 11.5, and 9.5% of variability, respectively, that is 61.1% of total variability (Online Resource 3).

The variables that contributed the most to the formation of the components were (Table 2): (i) for component 1: plant description variables, the major one was the number of determined axes, NbDetA (8.1%). The second largest variable was the number of short axes (NbSA; 8.0%); it was not selected because it belonged to the same category; (ii) for component 2: axis geometry variables, the branching angle of the cord of the short axes in relation to the vertical axis, AngSA (9.5%); (iii) for component 3: plant description variables, the number of order 3 short axes, NbSA3 (7.4%); axis morphology variables, the length of order 4 short axes, LSA4 (10.6%); and (iv) for component 4: axis morphology variables, the length of the long axes, LLA (9.6%); axis topology variables, the number of branches on the long axes in the distal zone, NbBrTopLA (12.2%).

Six variables were thus selected for further analysis: (i) at the plant scale, NbDetA and NbSA3; and (ii) at the axis scale, LLA, NbBrTopLA, LSA4, and AngSA. The four categories of architectural variables were represented.

Correlations between the six selected variables were calculated for each population and year.

For the 'The Fairy' × 'Old Blush' progeny, correlations between architectural variables measured in 2014 and 2015 varied from −0.15 (NbBrTopLA_14-AngSA_15) to 0.67 (NbSA3_14-NbSA3_15). Out of the 66 correlations, 31 were significantly correlated (Online Resource 4): (i) one was high ($r \geq |0.60|$; NbSA3_14-NbSA3_15); (ii) six were moderately correlated ($|0.40| < r < |0.60|$); they mainly involved the pair of variables NbSA3-NbDetA; and (iii) 24 were weakly correlated ($|0.17| \leq r \leq |0.40|$; NbDetA-NbBrTopLA, NbDetA-LLA, NbSA3-NbBrTopLA, and NbSA3-LLA).

For the 'The Fairy' × 'Perle d'Or' progeny, correlations between the architectural variables measured in 2014 and 2015 varied from −0.28 (NbSA3_14-LSA4_14) to 0.73 (NbBrTopLA_14-LLA_14). Out of the 66 correlations, 36 were significantly correlated (Online Resource 5): (i) two were high ($r \geq |0.60|$); they involved the pair of variables NbBrTopLA-LLA; (ii) four were moderately correlated ($|0.40| < r < |0.60|$; NbSA3-NbBrTopLA); and (iii) 30 were weakly correlated ($|0.17| \leq r \leq |0.40|$; NbSA3-NbDetA, NbSA3-LLA, and LLA-AngSA).

Table 3 Mean phenotypic values and standard deviations (SD) for the parents 'The Fairy', 'Old Blush', and 'Perle d'Or' and the value range for the progenies

Trait	'The Fairy'		'Old Blush'		'Perle d'Or'		'The Fairy' × 'Old Blush'		'The Fairy' × 'Perle d'Or'	
	2014	2015	2014	2015	2014	2015	2014	2015	2014	2015
NbDetA	63.1 (39.4)	34.9 (14.2)	19.3 (15.4)	14.7 (6.5)	13.3 (7.9)	13.6 (6.4)	7.0–85.3	8.0–73.5	5.3–133	1.33–132.0
NbSA3	8.1 (2.0)	6.2 (1.3)	1.1 (0.9)	1.0 (1.3)	1.3 (1.5)	1.1 (1.2)	1.3–7.3	1.0–8.0	1.0–11.0	0.0–9.0
LLA (cm)	24.2 (21.7)	22.2 (12.9)	17.9 (13.2)	20.7 (14.9)	19.8 (10.6)	13.7 (9.9)	14.6–45.5	15.2–31.1	6.9–47.4	7.1–40.0
NbBrTopLA	2.5 (2.5)	2.9 (2.1)	0.6 (1.1)	0.9 (1.5)	1.0 (1.0)	0.8 (0.9)	0.7–4.0	0.6–3.7	0.1–4.2	0.0–3.8
LSA4 (cm)	1.3 (1.4)	1.0 (0.8)	2.4 (1.9)	2.2 (1.5)	2.7 (2.9)	3.5 (2.1)	0.7–4.2	0.7–3.3	0.4–6.5	0.6–4.1
AngSA (°)	97.0 (40.1)	88.0 (35.9)	86.2 (40.5)	84.1 (36.0)	67.5 (29.4)	64.9 (33.7)	42.1–144.7	49.0–141.1	49.4–131.0	52.3–118.4
AngLA2 (°)	113.3 (24.2)	103.8 (11.2)	71.5 (22.0)	60.9 (26.8)	62.2 (25.6)	59.5 (14.4)	38.4–141.3	32.1–142.6	35.0–154.3	43.6–131.3

NbDetA, the number of determined axes; *NbSA3*, the number of order 3 short axes; *LLA*, the length of long axes; *NbBrTopLA*, the number of branchings on the long axes in the distal zone; *LSA4*, the length of the order 4 short axes; *AngSA*, the branching angle of the cord of the short axes in relation to the vertical axis; *AngLA2*, the branching angle of the cord of the order 2 long axes in relation to the vertical axis

As expected, most of the variables were weakly to moderately correlated with one another.

Effects of the genotype, the year, and their interaction

The significance of genotype and year effects and their interaction was evaluated for the six architectural variables selected.

All selected variables showed a transgressive segregation as compared to their parents, whatever the progeny, except for NbSA3 measured in 2014 for the 'The Fairy' × 'Old Blush' progeny (Online Resources 6, 7, 8, and 9; Table 3).

The linear model residuals were normally distributed for all the architectural variables, except for LLA and LSA4, whatever the progeny. After transformation, the residuals were normally distributed (Online Resources 10 and 11).

For the 'The Fairy' × 'Old Blush' progeny, the genotype and year effects were significant for all the architectural variables except ln(LSA4), for which the year effect was not significant (ANOVA, $p < 0.05$; Table 4).

Regarding the year effect, 2015 had a significantly lower effect than 2014, with differences of − 15.5% for NbDetA, − 5.7% for NbSA3, − 18.3% for LLA, − 7.7% for NbBrTopLA, and − 10.5% for AngSA (Table 5).

A significant $G \times Y$ interaction was shown for ln(LSA4) and AngSA (ANOVA, $p < 0.05$; Tables 4 and 5). It was due to opposite responses from some genotypes, with extreme amplitudes: − 69.6% (FOB64) and + 251.2% (FOB162) for LSA4; − 59.2% (FOB258) and + 177.0% (FOB228) for AngSA (data not shown).

For the 'The Fairy' × 'Perle d'Or' progeny, the genotype effect was significant for all the architectural variables (ANOVA, $p < 0.05$; Table 6).

A significant year effect was shown for ln(LLA) and AngSA, with − 9.0% for LLA and − 6.5% for AngSA in 2015 as compared to 2014 (Table 5).

Table 4 Combined analysis of variance of six architectural variables measured in 2014 and 2015 for the 'The Fairy' × 'Old Blush' progeny

Variables	Source of variation	*df*	Mean squares	*F* probability
NbDetA	Year (*Y*)	1	4795.7	**
	Genotype (*G*)	131	712.7	**
	$G \times Y$	130	277.4	NS
	Residuals	495	335.4	
NbSA3	Year (*Y*)	1	13.0050	*
	Genotype (*G*)	131	9.3683	**
	$G \times Y$	130	1.8698	NS
	Residuals	495	2.9138	
ln(LLA)	Year (*Y*)	1	37.656	**
	Genotype (*G*)	131	0.905	**
	$G \times Y$	130	0.604	NS
	Residuals	5067	0.541	
NbBrTopLA	Year (*Y*)	1	29.8137	**
	Genotype (*G*)	131	9.6543	**
	$G \times Y$	130	2.3855	NS
	Residuals	5067	3.6360	
ln(LSA4)	Year (*Y*)	1	0.0753	NS
	Genotype (*G*)	130	4.6678	**
	$G \times Y$	129	1.9663	**
	Residuals	9293	0.5727	
AngSA (°)	Year (*Y*)	1	447,005	**
	Genotype (*G*)	131	30,308	**
	$G \times Y$	130	29,246	**
	Residuals	17,039	1203	

NbDetA, the number of determined axes; *NbSA3*, the number of order 3 short axes; *LLA*, the length of long axes; *NbBrTopLA*, the number of branchings on the long axes in the distal zone; *LSA4*, the length of the order 4 short axes; *AngSA*, the branching angle of the cord of the short axes in relation to the vertical axis; *ln*, neperian logarithm; *df*, degrees of freedom

Significance of effects: *NS*, not significant; *, significant ($0.01 < p \leq 0.05$); **, highly significant ($p \leq 0.01$)

Table 5 Average values of the six architectural variables measured in 2014 and 2015

Variables	'The Fairy' × 'Old Blush'		'The Fairy' × 'Perle d'Or'	
	2014	2015	2014	2015
NbDetA	32.36	27.33	34.72	31.15
NbSA3	4.56	4.30	4.32	4.25
LLA (cm)	25.71	21.00	19.36	17.61
NbBrTopLA	1.95	1.80	1.59	1.61
LSA4 (cm)	1.92	1.73	1.58	1.49
AngSA (°)	97.18	86.94	94.24	88.13

NbDetA, the number of determined axes; *NbSA3*, the number of order 3 short axes; *LLA*, the length of long axes; *NbBrTopLA*, the number of branchings on the long axes in the distal zone; *LSA4*, the length of the order 4 short axes; *AngSA*, the branching angle of the cord of the short axes in relation to the vertical axis

A significant $G \times Y$ interaction was shown for NbSA3, ln(LLA), ln(LSA4), and AngSA (ANOVA, $p < 0.05$; Tables 5 and 6). It was due to opposite responses from some genotypes, with extreme amplitudes: − 100.0% (FPO06) and + 316.7% (FPO267) for NbSA3; − 61.7% (FPO06) and + 94.1% (FPO261) for LLA; − 78.1% (FPO413) and + 197.6% (FPO19) for LSA4; and − 39.6% (FPO402) and + 126.5% (FPO139) for AngSA (data not shown).

Table 6 Combined analysis of variance of six architectural variables measured in 2014 and 2015 for the 'The Fairy' × 'Perle d'Or' progeny

Variables	Source of variation	*df*	Mean squares	*F* probability
NbDetA	Year (*Y*)	1	2639.12	NS
	Genotype (*G*)	155	1668.70	**
	$G \times Y$	145	544.47	NS
	Residuals	526	701.08	
NbSABrO3	Year (*Y*)	1	0.8713	NS
	Genotype (*G*)	155	13.6901	**
	$G \times Y$	145	5.9143	**
	Residuals	526	4.3923	
ln(LLA)	Year (*Y*)	1	5.5862	**
	Genotype (*G*)	155	1.6178	**
	$G \times Y$	145	0.8194	**
	Residuals	6132	0.5674	
NbBrTopLA	Year (*Y*)	1	0.9710	NS
	Genotype (*G*)	155	7.2932	**
	$G \times Y$	145	3.4172	NS
	Residuals	6132	3.0758	
ln(LSA4)	Year (*Y*)	1	0.4811	NS
	Genotype (*G*)	154	4.4564	**
	$G \times Y$	143	2.0873	**
	Residuals	11,433	0.5186	
AngSA (°)	Year (*Y*)	1	193,813	**
	Genotype (*G*)	155	20,021	**
	$G \times Y$	154	15,251	**
	Residuals	20,543	1221	

NbDetA, the number of determined axes; *NbSA3*, the number of order 3 short axes; *LLA*, the length of long axes; *NbBrTopLA*, the number of branchings on the long axes in the distal zone; *LSA4*, the length of the order 4 short axes; *AngSA*, the branching angle of the cord of the short axes in relation to the vertical axis; *ln*, neperian logarithm; *df*, degrees of freedom

Significance of effects: *NS*, not significant; *, significant ($0.01 < p \leq 0.05$); **, highly significant ($p \leq 0.01$)

Broad-sense heritability

For each variable, phenotypic variance and its components, as well as heritability, are given in Tables 7 and 8.

For the 'The Fairy' × 'Old Blush' progeny, genotypic variance accounted for the major part of phenotypic variance, except for ln(LLA) (36.5%) and AngSA (3.5%). Genotypic variance was high (> 60%) for NbSA3 and NbBrTopLA, intermediate (between 40 and 60%) for NbDetA and ln(LSA4), low (between 20 and 40%) for ln(LLA), and very low (< 20%) for AngSA. The variance of the $G \times Y$ interaction was very high (> 80%) for AngSA and low for ln(LSA4). Consequently, residual variance was high for ln(LLA), intermediate for NbDetA, low for NbSA3 and NbBrTopLA, and very low for ln(LSA4) and AngSA. The broad-sense heritability values calculated for each of the variables were 0.71 for NbSA3, 0.63 for NbBrTopLA, 0.58 for ln(LSA4), 0.54 for NbDetA, 0.36 for ln(LLA), and 0.03 for AngSA.

For the 'The Fairy' × 'Perle d'Or' progeny, genotypic variance was intermediate for all variables, except for AngSA, which was low (23.8%). The variance of the $G \times Y$ interaction was high (> 60%) for AngSA, low for ln(LSA4), and very low for NbSA3 and ln(LLA). Consequently, residual variance was intermediate for NbDetA and NbBrTopLA, low for NbSA3 and ln(LLA), and very low for ln(LSA4) and AngSA. The broad-sense heritability values calculated for each of the variables were 0.59 for NbDetA, 0.58 for NbBrTopLA, 0.57 for NbSA3, 0.53 for ln(LSA4), 0.49 for ln(LLA), and 0.24 for AngSA.

The broad-sense heritability value of AngSA was very low, so it was replaced for further analysis by AngLA2, with which it was highly correlated ($0.67 \leq r \leq 0.80$, depending on the population and the year). The broad-sense heritability value of AngLA2 was moderate, ranging between 0.37 for the 'The Fairy' × 'Old Blush' progeny and 0.55 for the 'The Fairy' × 'Perle d'Or' progeny.

Genetic linkage maps

Each parental map consisted of seven LGs corresponding to the seven haploid rose chromosomes. Our genetic maps are comparable to the map developed by Kawamura et al. (2015). Two to nine SSR markers were common per LG. The numbers of LGs were assigned according to the rose consensus map of Spiller et al. (2011).

Table 7 Variance components and broad-sense heritability estimates of six architectural variables measured in 2014 and 2015 for the 'The Fairy' × 'Old Blush' progeny

Variance component and heritability	NbDetA	NbSA3	ln(LLA)	NbBrTopLA	ln(LSA4)	AngSA	AngLA2
Genotypic variance	67.0 (53.8)	1.16 (71.1)	0.008 (36.5)	0.15 (62.6)	0.037 (57.9)	8.1 (3.5)	117.0 (36.6)
Genotypic by year variance	–	–	–	–	0.019 (29.8)	213.9 (92.5)	118.1 (36.9)
Residual variance	57.5 (46.2)	0.47 (28.9)	0.014 (63.5)	0.09 (37.4)	0.008 (12.3)	9.2 (4.0)	84.4 (26.4)
Phenotypic variance	124.5	1.63	0.022	0.24	0.064	231.2	319.5
Heritability	0.54	0.71	0.36	0.63	0.58	0.03	0.37

Values in brackets are percentages over the phenotypic variance

NbDetA, the number of determined axes; *NbSA3*, the number of order 3 short axes; *LLA*, the length of long axes; *NbBrTopLA*, the number of branchings on the long axes in the distal zone; *LSA4*, the length of the order 4 short axes; *AngSA*, the branching angle of the cord of the short axes in relation to the vertical axis; *AngLA2*, the branching angle of the cord of the order 2 long axes in relation to the vertical axis; *ln*, neperian logarithm

Table 8 Variance components and broad-sense heritability estimates of six architectural variables measured in 2014 and 2015 for the 'The Fairy' × 'Perle d'Or' progeny

Variance component and heritability	NbDetA	NbSA3	ln(LLA)	NbBrTopLA	ln(LSA4)	AngSA	AngLA2
Genotypic variance	185.8 (59.5)	1.4 (56.8)	0.019 (49.3)	4.13 (57.8)	0.031 (53.2)	35.7 (23.8)	128.9 (55.0)
Genotypic by year variance	–	0.3 (11.1)	0.006 (15.6)	–	0.020 (35.2)	104.9 (70.1)	23.1 (9.9)
Residual variance	126.6 (40.5)	0.8 (32.1)	0.014 (35.1)	3.0 (42.2)	0.007 (11.6)	9.1 (6.1)	82.3 (35.1)
Phenotypic variance	312.4	2.5	0.039	7.1	0.059	149.8	234.3
Heritability	0.59	0.57	0.49	0.58	0.53	0.24	0.55

Values in brackets are percentages over the phenotypic variance

NbDetA, the number of determined axes; NbSA3, the number of order 3 short axes; *LLA*, the length of long axes; *NbBrTopLA*, the number of branchings on the long axes in the distal zone; *LSA4*, the length of the order 4 short axes; *AngSA*, the branching angle of the cord of the short axes in relation to the vertical axis; *AngLA2*, the branching angle of the cord of the order 2 long axes in relation to the vertical axis; *ln*, neperian logarithm

'The Fairy' × 'Old Blush' maps

A total of 56 and 55 SSR and gene markers were used to construct the female and male maps of 'The Fairy' and 'Old Blush', respectively. The maps covered 267.5 cM for 'The Fairy' and 310.8 cM for 'Old Blush'. The number of markers ranged from 6 to 11 per LG. The average distance between markers was 4.2 cM for 'The Fairy' and 5.7 cM for 'Old Blush'. The largest gaps were 25.8 cM on LG5 for 'The Fairy' and 43.6 cM on LG5 for 'Old Blush'. Distorted markers were mainly assigned to LG2 for 'The Fairy', with a total percentage of distortion of 14.3%, and to LGs 1, 2, 3, and 7 for 'Old Blush', with a total percentage of distortion of 63.0%.

'The Fairy' × 'Perle d'Or' maps

A total of 55 and 49 SSR and gene markers were used to construct the female and male maps of 'The Fairy' and 'Perle d'Or', respectively. The maps covered 289.8 cM for 'The Fairy' and 354.6 cM for 'Perle d'Or'. The number of markers ranged from 4 to 11 per LG. The average distance between markers was 5.3 cM for 'The Fairy' and 7.2 cM for 'Perle d'Or'. The largest gaps were 30.4 cM on LG5 for 'The Fairy' and 43.0 cM on LG5 for 'Perle d'Or'. Distorted markers were mainly assigned to LGs 2 and 5 for 'The Fairy', with a total percentage of distortion of 32.7%, and to all LGs except LG5 for 'Perle d'Or', with a total percentage of distortion of 71.4%.

QTL analysis

For the 'The Fairy' × 'Old Blush' progeny, QTL analysis revealed a total of 37 QTLs, the two years taken together (Table 9): 17 on the female map of 'The Fairy' and 20 on the male map of 'Old Blush'; they were distributed on all LGs except on LG4. For the 'The Fairy' × 'Perle d'Or' progeny, 14 QTLs were detected (Table 10): four on the female map of 'The Fairy' and 10 on the male map of 'Perle d'Or'; they were located mainly on LGs 2, 4, and 7. No QTLxQTL interaction was revealed, whatever the variable.

Number of determined axes (NbDetA)

Two QTLs were detected on 'Old Blush' LGs 5 and 6, and one on 'Perle d'Or' LG2 in 2014, and accounted for 16.5, 8.1, and 16.8% of NbDetA variability, respectively (Table 9). Only 'Perle d'Or' LG2 QTL was detected in 2015 (a stable QTL), when it accounted for 18.5% of total variability (Table 10).

Number of order 3 short axes (NbSA3)

For the 'The Fairy' × 'Old Blush' progeny, two QTLs were detected on 'The Fairy' LGs 1 and 2, and one on 'Old Blush' LG2 in 2014, and explained 9.1, 9.9, and 13.3% of NbSA3 variability, respectively. In 2015, 'The Fairy' and 'Old Blush' LG2 QTLs were once again detected (stable QTLs), as well as one additional QTL on 'Old Blush' LG7. They explained 14.2, 13.3, and 10.1% of total variability, respectively (Table 9).

For the 'The Fairy' × 'Perle d'Or' progeny, one QTL was also detected on 'The Fairy' LG2 in 2014 and one on 'Perle d'Or' LG2 in 2015, explaining 7.8 and 9.3% of NbSA3 variability, respectively. Only one QTL was detected for the BLUP of the genotype and $G \times Y$ effects. It was located on 'Perle d'Or' LG2 and explained 8.6% of NbSA3_BLUP and 6.8% of NbSA3_BLUP_15, respectively (Table 10). For this trait, all LG2 QTLs were detected in the same region and co-located with QTLs for NbDetA (Fig. 3).

Length of long axes (LLA)

For the 'The Fairy' × 'Old Blush' progeny, one QTL was detected on 'The Fairy' LG2, and one on 'Old Blush' LG7 in 2014, and explained 10.4 and 9.9% of ln(LLA) variability, respectively (Table 9). 'Old Blush' LG7 QTL co-localized with *RhBRC1*, a repressor of branching (Barbier et al. 2015). QTLs for NbSA3 and AngLA2 were also located in the same genomic regions (Fig. 2).

For the 'The Fairy' × 'Perle d'Or' progeny, two QTLs were detected for the BLUP of the genotype effect. They were located on 'Perle d'Or' LGs 4 and 7 and explained 10.4 and 8.0% of total variability, respectively. No year-specific QTL was detected for the BLUP of the $G \times Y$ effect (Table 10).

Number of branchings on the long axes in the distal zone (NbBrTopLA)

Only one QTL was detected on 'Old Blush' LG6 in 2014 and explained 15.8% of NbBrTopLA variability. In 2015, 'Old Blush' LG6 QTL was once again detected (a stable QTL), as well as two additional QTLs on 'Old Blush' LG5 and 'Perle d'Or' LG2. They explained 13.5, 10.3, and 8.1% of total variability, respectively (Table 9). These QTLs were located nearby NbDetA QTLs (Fig. 2).

Length of the order 4 short axes (LSA4)

For the 'The Fairy' × 'Old Blush' progeny, two QTLs were detected on 'The Fairy' LGs 2 and 5 and one on 'Old Blush' LG1 for the BLUP of the genotype effect. They explained 10.1, 9.6, and 9.5% of ln(LSA4_BLUP) variability, respectively. Only one QTL was detected on 'The Fairy' LG5 in 2014 and explained 8.8% of ln(LSA4) variability. No year-specific QTL was detected for the BLUP of the $G \times Y$ effect (Table 9).

Table 9 Parameters associated with the quantitative trait loci (QTLs) detected in the 'The Fairy' × 'Old Blush' progeny for the six architectural traits selected

Trait	'The Fairy'								'Old Blush'							
	LG	Position (cM)	Interval[a]	Locus	LOD[b]	R^{2c}	Global R^{2d}	D^{e} (%)	LG	Position (cM)	Interval	Locus	LOD	R^2	Global R^2	D (%)
NbDetA_14	No QTL								5	43.6	36.0–45.0	RMS034	6.0	16.5	29.5	−33.5
									6	0.0	0.0–14.0	H22E04	3.1	8.1		−27.9
NbDetA_15	No QTL								No QTL							
NbSA3_14	1	15.0	7.0–23.0	H23017	3.0	9.1	18.6	−5.8	2	12.9	11.0–15.0	CTG172	4.0	13.3	13.3	−29.3
	2	30.0	14.0–47.0	RMS137	3.3	9.9		+19.7								
NbSA3_15	2	19.0	12.0–34.0	Rw23F13	4.4	14.2	14.2	+32.6	2	12.9	11.0–14.0	CTG172	4.8	13.3	27.4	−36.2
									7	35.0	29.0–40.5	H10D03	3.7	10.1		−22.1
ln(LLA_14)	2	36.0	31.0–54.0	RMS129	3.1	10.4	10.4	−6.4	7	39.0	26.0–40.5	*RhBRC1*	3.0	9.9	9.9	+9.1
ln(LLA_15)	No QTL								No QTL							
NbBrTopLA_14	No QTL								6	12.0	5.0–18.0	RMS108	4.9	15.8	15.8	+26.7
NbBrTopLA_15	No QTL								5	53.6	44.0–62.0	H17C12	3.7	10.3	26.3	−21.9
									6	9.0	3.0–16.0	RMS108	4.8	13.5		+28.3
ln(LSA4_14)	5	23.0	12.0–30.1	Rw10J19	2.6	8.8	8.8	+22.2	No QTL							
ln(LSA4_15)	No QTL								1	0.0	0.0–2.0	RhAB9	2.7	9.2	9.2	+12.5
ln(LSA4_BLUP)	2	38.0	32.0–54.0	RMS129	3.4	10.1	20.9		1	21.0	0.0–27.0	H9B07	2.8	9.5	9.5	
	5	18.0	8.0–28.0	Rw10J19	3.2	9.6										
ln(LSA4_BLUP_14)	No QTL								No QTL							
ln(LSA4_BLUP_15)	No QTL								No QTL							
AngLA2_14	2	54.0	47.0–60.0	Rw54N22	3.3	10.0	20.0	+20.1	No QTL							
	6	0.0	0.0–1.0	H22E04	2.6	7.7		−16.3								
AngLA2_15	2	67.7	64.0–67.7	CTG356	4.6	13.5	22.1	+21.2	2	16.6	15.0–21.0	Rw3K19	3.4	8.2	35.0	−7.0
	5	2.4	0.0–8.0	RMS034	3.3	9.7		+18.8	5	46.0	43.6–50.0	Rw14H21	5.2	12.9		−15.8
									7	38.0	33.0–40.5	*RhBRC1*	7.1	18.4		−18.6
AngLA2_BLUP	2	57.0	52.0–59.0	Rw54N22	8.0	19.5	39.5		1	22.8	19.0–26.0	H9B07	3.8	8.7	38.2	
	3	11.0	3.0–19.5	Rw12J12	3.2	7.3			2	16.9	16.1–20.0	RMS132	3.6	8.3		
	5	2.4	1.0–10.0	RMS034	3.7	8.5			5	48.0	44.0–51.0	H24D11	4.5	10.5		
	6	0.0	0.0–1.0	H22E04	4.1	9.3			7	40.5	36.0–40.5	*RhBRC1*	7.0	17.0		
AngLA2_BLUP_14	No QTL								No QTL							
AngLA2_BLUP_15	2	67.6	23.0–67.6	CTG356	3.1	9.6	17.5		5	62.0	27.0–80.0	H17C12	2.6	7.2	23.5	
	5	2.4	0.0–15.0	RMS034	2.9	8.8			7	36.0	24.0–40.4	H10D03	5.4	15.8		

The QTL detection was carried out for each trait in 2014 and 2015; the year is indicated at the end of the trait: 14 for 2014 and 15 for 2015. BLUP (best linear unbiased predictor) and BLUP followed by the year indicate QTLs detected for the genotype effect and the genotype × year effect, respectively

NbDetA, the number of determined axes; *NbSA3*, the number of order 3 short axes; *LLA*, the length of long axes; *NbBrTopLA*, the number of branchings on the long axes in the distal zone; *LSA4*, the length of the order 4 short axes; *AngLA2*, the branching angle of the cord of the order 2 long axes in relation to the vertical axis; *ln*, neperian logarithm

[a] 1-LOD interval cM

[b] Maximum logarithm of the odds (LOD) score value of the QTL

[c] Percentage of the phenotypic variation explained by each term of model, i.e., QTL

[d] Percentage of the phenotypic variation explained by the whole model

[e] Difference in the phenotype between marker alleles (for the heterozygous genotype, lm, compared to homozygous, ll)

Table 10 Parameters associated with the quantitative trait loci (QTLs) detected in the 'The Fairy' × 'Perle d'Or' progeny for the six architectural traits selected

Trait	'The Fairy'								'Perle d'Or'							
	LG	Position (cM)	Interval[a]	Locus	LOD[b]	R^{2c}	Global R^{2d}	D^{e} (%)	LG	Position (cM)	Interval	Locus	LOD	R^2	Global R^{2d}	D (%)
NbDetA_14	No QTL								2	46.0	40.0–56.0	RMS137	6.2	16.8	16.8	+65.9
NbDetA_15	No QTL								2	43.0	37.0–50.0	RMS137	6.5	18.5	18.5	+75.7
NbSA3_14	2	16.0	12.0–21.0	RMS082	2.7	7.8	7.8	+56.1	No QTL							
NbSA3_15	No QTL								2	47.0	38.0–62.0	RMS137	3.1	9.3	9.3	+33.7
NbSA3_BLUP	No QTL								2	83.0	39.0–91.0	RMS132	3.0	8.6	8.6	
NbSA3_BLUP_14	No QTL								No QTL							
NbSA3_BLUP_15	No QTL								2	50.0	32.0–91.0	RMS137	2.2	6.8		
ln(LLA_14)	No QTL								No QTL							
ln(LLA_15)	No QTL								No QTL							
ln(LLA_BLUP)	No QTL								4	31.0	24.0–38.4	CL3881	4.0	10.4	16.4	
									7	25.0	18.0–32.6	RMS066	3.1	8.0		
ln(LLA_BLUP_14)	No QTL								No QTL							
ln(LLA_BLUP_15)	No QTL								No QTL							
NbBrTopLA_14	No QTL								No QTL							
NbBrTopLA_15	No QTL								2	61.0	34.0–74.0	CL2996	2.7	8.1	8.1	+24.1
ln(LSA4_14)	No QTL								2	29.7	22.0–39.0	Rw29B1	3.1	8.7	8.7	−16.7
ln(LSA4_15)	No QTL								No QTL							
ln(LSA4_BLUP)	No QTL								2	31.0	27.3–40.0	Rw29B1	4.3	12.0	12.0	
ln(LSA4_BLUP_14)	No QTL								No QTL							
ln(LSA4_BLUP_15)	No QTL								No QTL							
AngLA2_14	2	49.0	43.0–53.9	Rh80	4.0	11.3	11.3	−11.2	No QTL							
AngLA2_15	2	53.9	46.0–53.9	Rw54N22	4.3	12.6	12.6	−16.0	No QTL							
AngLA2_BLUP	2	50.0	45.0–53.9	Rh80	6.0	16.4	16.4		No QTL							
AngLA2_BLUP_14	No QTL								No QTL							
AngLA2_BLUP_15	No QTL								No QTL							

The QTL detection was carried out for each trait in 2014 and 2015; the year is indicated at the end of the trait: 14 for 2014 and 15 for 2015. BLUP (best linear unbiased predictor) and BLUP followed by the year indicate QTLs detected for the genotype effect and the genotype × year effect, respectively

NbDetA, the number of determined axes; *NbSA3*, the number of order 3 short axes; LLA, the length of long axes; *NbBrTopLA*, the number of branchings on the long axes in the distal zone; *LSA4*, the length of the order 4 short axes; *AngLA2*, the branching angle of the cord of the order 2 long axes in relation to the vertical axis; *ln*, neperian logarithm

[a] 1-LOD interval cM

[b] Maximum logarithm of the odds (LOD) score value of the QTL

[c] Percentage of the phenotypic variation explained by each term of model, i.e., QTL

[d] Percentage of the phenotypic variation explained by the whole model

[e] Difference in the phenotype between marker alleles (for the heterozygous genotype, lm, compared to homozygous, ll)

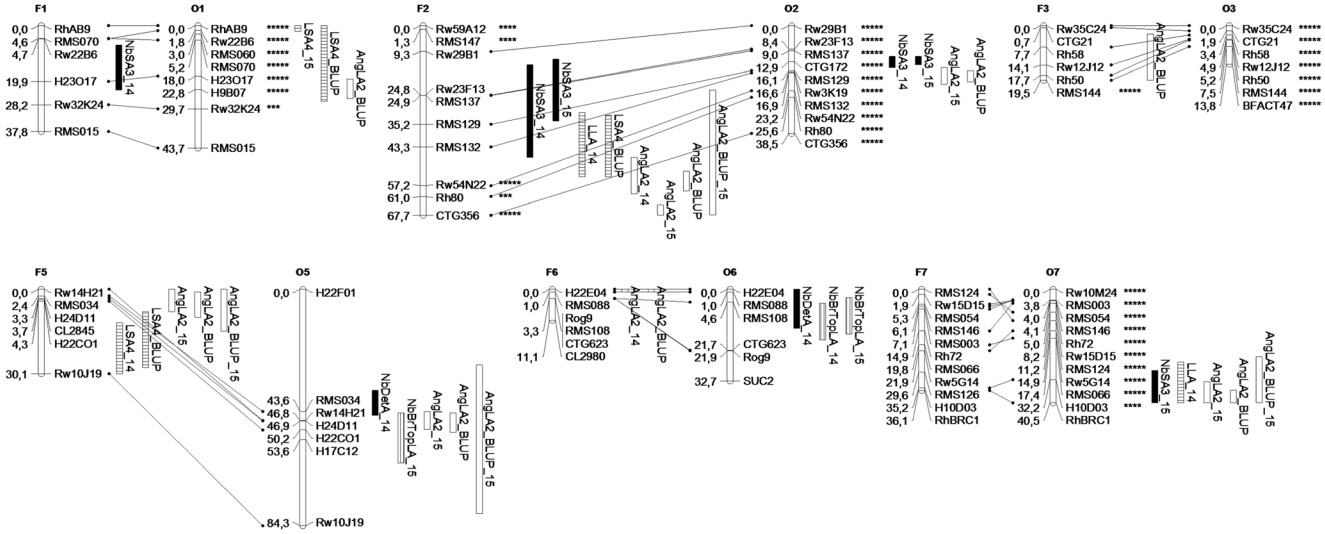

Fig. 2 Genomic positions of quantitative trait loci (QTLs) detected on the linkage groups (LGs) 1, 2, 3, 5, 6, and 7 of the 'The Fairy' female map (F) and 'Old Blush' male parent map (O) for the six architectural variables selected. The LGs are numbered according to Spiller et al. (2011). QTLs are represented on the right side of LGs by boxes; their length represents the LOD-1 confidence interval. Boxes representing QTLs for plant description traits are in black, axis morphology traits are horizontally hatched, axis topology traits are vertically hatched, and axis geometry traits are white. For trait abbreviations, see Table 2. Marker distortion was tested against the expected Mendelian ratios using the chi-square test. Marker segregation distortions are indicated on the right of the marker (***$p < 0.01$; ****$p < 0.001$; *****$p < 0.0001$)

For the 'The Fairy' × 'Perle d'Or' progeny, only one QTL was detected on 'Perle d'Or' LG2 for the BLUP of the genotype effect. It explained 12.0% of ln(LSA4_BLUP) variability. This QTL was only detected in 2014, when it explained 8.7% of total variability. No year-specific QTL was detected for the BLUP of the $G \times Y$ effect (Table 10). For this trait, QTLs were detected nearby NbDetA and NbSA3 QTLs (Fig. 3).

Branching angle of the cord of the order 2 long axes in relation to the vertical axis (AngLA2)

For the 'The Fairy' × 'Old Blush' progeny, four QTLs were detected on 'The Fairy' LGs 2, 3, 5, and 6 for the BLUP of the genotype effect and explained 19.5, 7.3, 8.5, and 9.3% of AngLA2_BLUP variability, respectively. Out of these QTLs, one QTL was detected on LG2 in 2014, explaining 10.0% of total variability. LG6 and LG5 QTLs were only detected in 2014 and 2015, respectively, and explained 7.7 and 9.7% of variability. Two 2015 specific QTLs were detected on LG2 and LG5 for the BLUP of the $G \times Y$ effect and explained 9.6 and 8.8% of AngLA2_BLUP_15 variability. These QTLs were co-localized with AngLA2_15 QTLs (Table 9; Fig. 2).

Likewise, four QTLs were detected on 'Old Blush' LGs 1, 2, 5, and 7 for the BLUP of the genotype effect and explained 8.7, 8.3, 10.5, and 17.0% of AngLA2_BLUP variability, respectively. Out of these QTLs, only LGs 2 and 5 and 7 QTLs were detected in 2015, explaining 8.2, 12.9, and 18.4% of total variability, respectively. These QTLs were located nearby NbSA3 and LSA4 QTLs, while LG7 QTL co-localized with *RhBRC1*. Two 2015 specific QTLs were detected on LG5 and LG7 for the BLUP of the $G \times Y$ effect and explained

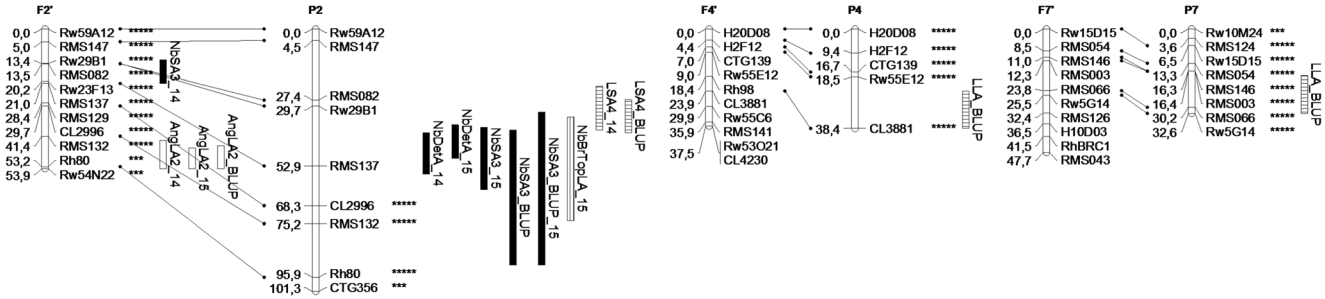

Fig. 3 Genomic positions of quantitative trait loci (QTLs) detected on the linkage groups (LGs) 2, 4, and 7 of the 'The Fairy' female map (F′) and 'Perle d'Or' male parent map (P) for the six architectural variables selected. The LGs are numbered according to Spiller et al. (2011). QTLs are represented on the right side of LGs by boxes; their length represents the LOD-1 confidence interval. Boxes representing QTLs for plant description traits are in black, axis morphology traits are horizontally hatched, axis topology traits are vertically hatched, and axis geometry traits are white. For trait abbreviations, see Table 2. Marker distortion was tested against the expected Mendelian ratios using the chi-square test. Marker segregation distortions are indicated on the right of the marker (***$p < 0.01$; ****$p < 0.001$; *****$p < 0.0001$)

7.2 and 15.8% of AngLA2_BLUP_15 variability. These QTLs were co-localized with AngLA2_15 QTLs (Table 9; Fig. 2).

For the 'The Fairy' × 'Perle d'Or' progeny, one QTL was detected on 'The Fairy' LG2 for the BLUP of the genotype effect. It explained 16.4% of AngLA2_BLUP variability. This QTL was detected in 2014 and 2015 (a stable QTL) and explained 11.3 and 12.6% of total variability, respectively (Table 10). For this trait, all the 'The Fairy' LG2 QTLs were detected in the same genomic region (Fig. 3).

Discussion

Selecting the most relevant variables

The phenotyping of plant architecture by 3D digitalization allowed us to access a set of variables corresponding to the four categories defined by Crespel et al. (2013): at the plant scale, the first category of variables primarily focused on the number of axes and differentiated between short and long axes; at the axis scale, the other three categories of variables focused on morphology, topology, and geometry. As a result, an almost exhaustive description of rose bush architecture was obtained and generated 41 variables. A similar phenotyping approach had been used by Segura et al. (2006, 2007) for the genetic analysis of apple tree architecture.

In order to avoid any redundant information, the genetic analysis was performed on the most relevant variables—the ones that were most explanatory of phenotypic variability and least correlated. To select them, a PCA was carried out on the 41 architectural variables. Based on their contribution to the formation of the first four components of the PCA, the number of variables was reduced from 41 to six. This reduction was done with respect for the breakdown of variables by category, as defined above.

Out of the six variables we selected, five had never been analyzed genetically from segregating, recurrent blooming populations. Most of them were inaccessible manually, i.e., at the plant scale, the number of determined axes (NbDetA) and the number of order 3 short axes (NbSA3), and at the axis scale, the length of the long axes (LLA), the number of branches on the long axes in the distal zone (NbBrTopLA), and the length of the order 4 short axes (LSA4).

The correlations between the six variables were mostly low to moderate. However, a strong correlation was observed between NbBrTopLA and LLA ($r = 0.73$ in 2014 and $r = 0.70$ in 2015) for the 'The Fairy' × 'Perle d'Or' progeny, highlighting a relationship between the number of branches and the length of the bearing axis. Likewise, most moderate correlations were observed between the variables NbSA3-NbDetA and NbSA3-NbBrTopLA. The proportion of short axes is higher in rose bush as compared to long axes (Morel et al. 2009); therefore, NbDetA and NbBrTopLA are believed to involve mainly this type of axis.

Effects of the genotype, the year, and their interaction

For the 'The Fairy' × 'Old Blush' progeny, a significant year effect was observed for all variables, with lower values for 2015 than for 2014, except for ln(LSA4). A greater phenotypic plasticity of traits was observed for this progeny as compared to the 'The Fairy' × 'Perle d'Or' progeny, for which a significant year effect was only shown for ln(LLA) and AngSA. The year effect was more pronounced for NbDetA (− 15.5% for 2015 as compared to 2014). The total number of determined axes is dependent on the degree of branching of the long axes (Crespel et al. 2014), so the difference observed between 2014 and 2015 could be due to a reduction in the number of bud breaks on the first order axes in 2015 caused by the lower amount of radiation received by the plants in March (− 26.4% as compared to 2014). This reduction in the number of branches was significant for the short axes (SAs)—contrary to the long axes (LAs)—whatever the branching order from branching order 3 to 5 (data not shown), with − 5.7% for NbSA3. This relationship between the number of axes produced and the amount of radiation was largely described by Zieslin and Mor (1990), and more recently by Leduc et al. (2014). This could also explain the significant reduction observed for NbBrTopLA (− 7.7%).

The year effect was also significant for the length of LAs (ln(LLA); − 18.3% for the 'The Fairy' × 'Old Blush' progeny and − 9.0% for 'The Fairy' x' Perle d'Or' for 2015 as compared to 2014). LAs are located at the level of first orders (Morel et al. 2009), so that they mainly developed in March and lengthened in April. The difference in length observed between 2014 and 2015 could be due to the higher amount of radiation received by the plants in April 2015 (+ 5.3%). This observation, which links length to the amount of radiation, is consistent with that of Bredmose (1998). He noted a significant reduction (− 5.8%) in axis length along with a 15.2% increase in daily radiation. Similar results were observed by Crespel et al. (2014) in rose bush.

The year effect was also significant for the branching angle of the short axes (AngSA); axes were more upright (− 10.5% for the 'The Fairy' × 'Old Blush' progeny and − 6.5% for 'The Fairy' x' Perle d'Or') in 2015, leading to a more orthotropic growth habit of the plants. Branching is mainly distal in rose bush (Morel et al. 2009). Thus, the difference observed between 2014 and 2015 for AngSA could be due to the lower load borne by the long axes, caused by the lower degree of branching in 2015, as was shown by Alméras et al. (2004) in apricot tree and suggested by Crespel et al. (2014) in rose bush.

A significant $G \times Y$ effect was shown for ln(LSA4) and AngSA, whatever the progeny, and for NbSA3 and ln(LLA)

in the 'The Fairy' × 'Perle d'Or' progeny. This interaction was due to opposite responses from some genotypes. A significant $G \times Y$ interaction was also shown by Crespel et al. (2014) for all the architectural variables measured in rose bush.

Broad-sense heritability

The broad-sense heritability (i.e., relative genotypic variance) ranged from very low to high for the 'The Fairy' × 'Old Blush' progeny, i.e., from 0.03 for AngSA to 0.71 for NbSA3, while it was low to moderate for the 'The Fairy' × 'Perle d'Or' progeny, ranging from 0.24 for AngSA to 0.59 for NbDetA. The relative genotypic variance was also low to moderate for the architectural variables of the flowering axis measured on a progeny resulting from the cross between 'The Fairy' and a hybrid of *R. wichurana* (Kawamura et al. 2011, 2015). It varied from 30.5% for the elevation angle of the order 2 axes to 62.7% for the number of nodes on the vegetative part of the order 1 axes. In all cases, the lowest heritability values were observed for the geometrical variables (i.e., the branching angle of the axes); they were particularly low in our study, so that genetic analysis was irrelevant. However, other geometrical variables correlated with AngSA were characterized by higher heritability; it was the case of AngLA2, with moderate heritability varying from 0.37 for the 'The Fairy' × 'Old Blush' progeny to 0.55 for the 'The Fairy' × 'Perle d'Or' progeny. Therefore, this variable was selected to replace AngSA for the rest of the study.

Broad-sense heritability depends on the progeny and the environment (Souza et al. 1998). For example, in the case of the progeny of a cut flower rose grown in various environments, the broad-sense heritability of architectural variables was higher than in our study, ranging from 0.40 for the number of branches to 0.84 for axis length (Gitonga et al. 2014). Similarly, in a range of eight rose bush cultivars with contrasting shapes, heritability values varied from 0.48 for the length of the long axes to 0.98 for the number of metamers of the long axes (Crespel et al. 2014). These greater heritability values could be explained by greater architectural variability among genotypes, as suggested by Segura et al. (2006) in apple tree. However, compared with our study, heritability values were in the same order of magnitude for the number of determined axes. The estimation of the heritability could be consolidated by the application of a broader range of contrasted environments by modulating factors that influence plant architecture such as light and water.

QTL analysis

The lengths of the parental genetic maps varied from 267.5 cM for the female map of 'The Fairy' to 354.6 cM for the male map of 'Perle d'Or'; they were smaller than in other studies, with a length of the rose genome estimated at 500 cM by Yan et al. (2005). This difference could be partly explained by the high percentage of distorted markers used for the construction of our genetic maps, ranging up to 71.4% for the male map of 'Perle d'Or'; the distortion of segregation is known to impact the estimate of genetic distances (Lorieux et al. 1995a, b).

High percentages of distorted markers were already reported in rose bush; they can vary from 22.0 to 41.0% ($p \leq 0.05$) (Yan et al. 2005; Moghaddam et al. 2012). Distortions of segregation were most commonly explained by pre- and/or postzygotic selection. In our study, the rate of seedling survival being high, postzygotic selection is unlikely to have occurred. However, sources of unintentional seedling selection caused by putative low vigor cannot be excluded. Nevertheless, the percentage of distortions was higher in the male (ranging from 63.0% for 'Old Blush' to 71.4% for 'Perle d'Or') than in the female parent (ranging from 14.3 to 32.7% for 'The Fairy'), suggesting the occurrence of male gametic selection. Distortions of segregation in rose bush could be due to a gametophytic self-incompatibility system, as early shown by Debener et al. (2010) in a progeny of *R. multiflora* hybrids—with the detection of a self-incompatibility (SI) gene on LG3—and suggested by Spiller et al. (2011). Distortions of segregation could also result from the genetic divergence between the parents and, therefore, the interspecific nature of progenies, as discussed by Dai et al. (2017).

For QTL analysis, the distortion of segregation only has a limited impact on QTL detection power and the estimate of its effects, provided that the distorted marker is not closely related to the QTL (Zhang et al. 2010). For the 'The Fairy' × 'Old Blush' progeny, QTL analysis revealed a total of 37 QTLs, the two years taken together: 17 on the female map of 'The Fairy' and 20 on the male map of 'Old Blush'. Both parents contributed to the control of architecture. Apart from LG1, the genomic regions involved in the control of architecture were homologous with Kawamura et al. (2011, 2015). They were distributed on all the chromosomes except on LG4. By contrast, QTLs were detected on this LG by Kawamura et al. (2011, 2015).

In our study, QTLs were more particularly located on LGs 2, 5, and 6; the weak to moderate correlations between variables cannot completely explain this. Among the QTLs we detected, 13 were major ($R^2 \geq 10\%$), with four of them located on LG2 from the female map of 'The Fairy' and nine on LGs 2, 5, 6, and 7 of the male map of 'Old Blush'. Major QTLs involved in the control of the plant shape and other architectural variables were also detected on LGs 2 and 6 by Yan et al. (2007), Djennane et al. (2013), and Kawamura et al. (2015). We detected major QTLs located on these LGs in 2014 and 2015; therefore, they were stable.

The number of QTLs detected per variable varied between two for ln(LLA) and seven for AngLA2, similar to Kawamura et al. (2011, 2015) who found numbers ranging from two for

the number of nodes on the longest 2 order axis which develops from the flowering part of the order 1 axis to six for plant shape. For the branching angle of the axes, we detected five new QTLs located on LGs 2, 6, and 7, compared to Kawamura et al. (2015). More interestingly, we also found that the QTL located on LG7 co-localized with *RhBRC1*, a branching repressor (Barbier et al. 2015) believed to play a central role in the integration of endogenous and exogenous signals (i.e., environmental factors; Teichmann and Muhr 2015) and explaining 18.4% of variability. This is consistent insofar as the number of branches borne by the axis is expected to influence its branching angle in rose bush (Crespel et al. 2014). In accordance with this, we found that AngLA2 and NbSA3 were correlated, with a common QTL located in the genomic region of *RhBRC1*. Compared to the map built by Kawamura et al. (2015), the QTLs detected on LGs 1 and 2 for NbSA3 could co-locate with *RwMAX3* and *RwMAX2*, two candidate genes involved in the biosynthesis and signaling pathway of strigolactones (SLs). This co-localization would be no surprise because SLs are involved in the control of bud break (Gomez-Roldan et al. 2008; Umehara et al. 2008) and are thought to transcriptionally control *BRC1* (Rameau et al. 2015). Co-localization (R^2 = 35.9%) between a major QTL involved in the control of branching intensity and *RwMAX2* was recently revealed in rose bush (Djennane et al. 2013). We evidenced that other QTLs located on LGs 5 and 6 could also be involved in the control of branching. They could co-locate with other genes involved in the strigolactone pathway, *RwMAX1* and *RwMAX4*, located on LG6 (Djennane et al. (2013). Similar results were obtained recently regarding the control of branching in chrysanthemum (Klie et al. 2015).

Besides the major QTL detected on LG2, we also found that a QTL located on LG7 co-localized with *RhBRC1* for ln(LLA). This seems to be consistent with the fact that *BRC1* can also inhibit cell division (Aguilar-Martinez et al. 2007; Teichmann and Muhr 2015) and, consequently, axis elongation, highlighting its pleiotropic character. Three QTLs were previously detected for stem length in rose bush, with a major one (R^2 = 35.0%) located on LG2 (Yan et al. 2007).

For variables ln(LSA4) and AngLA2, the effect of the $G \times Y$ interaction was significant, so we calculated the average value per genotype, adjusted it for the year effect, i.e., the BLUP for the genotype effect, and used it for new QTL detection. This approach had already been applied in apple tree (Celton et al. 2011). It revealed three QTLs independent of the year effect for ln(LSA4_BLUP), with a new QTL located on 'The Fairy' LG2, and eight QTLs for AngLA2_BLUP, with two new QTLs, located on 'The Fairy' LG3 and one on 'Old Blush' LG1.

Likewise, we calculated the BLUP for the $G \times Y$ effect. Thus, four 2015 specific QTLs were detected for AngLA2. They were located on 'The Fairy' LG2 and LG5, and 'Old Blush' LG5 and LG7, nearby *RhBRC1*, the expression of which is controlled by the environment (Aguilar-Martinez et al. 2007; Finlayson et al. 2010; Rameau et al. 2015).

For the 'The Fairy' × 'Perle d'Or' progeny, a lower number of QTLs was detected (a total of 13 QTLs, the two years taken together). The number of QTLs detected for a given character can differ between connected populations in corn (Meyer et al. 2007; Li et al. 2009) and in oil palm (Billotte et al. 2010). In our study, the female parent 'The Fairy' was common to both progenies, so that the less polymorphic QTLs of the male parent 'Perle d'Or' could explain this difference. However, we detected a much lower number of QTLs (between three and four times less as compared to the 'The Fairy' × 'Old Blush' progeny) on the female map of 'The Fairy'; these discrepancies in QTL detection between the two progenies could be due to the genetic background. They could result from epistatic interactions between QTLs, as shown by Meyer et al. (2007) and Li et al. (2009) in corn. Yet, all the QTLs we detected on the female map of 'The Fairy' were common to the 'The Fairy' × 'Old Blush' progeny. Most of them had a major effect and were located on LG2. Only one or two common QTLs were detected between connected populations by Meyer et al. (2007) and Li et al. (2009) in corn, as well as by Billotte et al. (2010) in oil palm. As in our study, most of these QTLs had a major effect.

We detected new QTLs involved in the control of NbDetA, NbBrTopLA, and ln(LSA4), all located on LG2 of the male map of 'Perle d'Or', an LG of interest for the control of rose bush architecture.

Taking into account the year effect, as previously for the 'The Fairy' × 'Old Blush' progeny, we detected two new QTLs for ln(LLA_BLUP) located on LGs 4 and 7. A comparison with the map built by Kawamura et al. (2015) showed that the QTL located on LG4 co-located with *Flowering locus T* (*RoFT*), a floral integrator, and was common with a QTL involved in the control of plant height. Kawamura et al. (2011) and Roman et al. (2015) showed that *RoFT* was involved in the control of the flowering date in rose bush. Stem length is indeed correlated with the number of days between bud break and flowering (i.e., the flowering date) in rose bush. It not only depends on light intensity and quality, but also on the temperatures applied during growth. A rise in temperature from 15 to 30 °C led to a reduction of stem length from 60.1 to 29.5 cm and of the number of days between bud break and flowering from 63.0 to 21.6 days (Shin et al. 2001). For the second QTL, a comparison with the male map of 'Old Blush' showed that it co-located with *RhBRC1*. BRC1 is known to interact with FT to prevent the early floral transition of axillary meristems, and thereby delay the date of flowering (Niwa et al. 2013).

To conclude, the analysis of the plant architecture by 3D digitalization made it possible to phenotype a large number of variables (41), most of them original because they were manually inaccessible. To avoid any redundant information in the analysis, we sorted the variables and kept the most

explanatory of the variability observed and least correlated ones. Thus, we selected six variables, five of which had never been analyzed genetically. The broad-sense heritability of most of these variables was moderate to high; therefore, their genetic analysis was consistent. It was, however, low for the geometrical variable, AngSA. It was replaced by a correlated variable, with moderate heritability: AngLA2. The geometrical variables being correlated with one another, another approach for QTL detection could be proposed: a joint analysis of these correlated variables (Banerjee et al. 2008). By including information from all variables, it should help to increase the QTL detection power and the precision of the estimated QTL effects for this category of variable, with low heritability.

The use of connected populations for the genetic analysis of these variables made it possible to detect a large number of QTLs, due to the broadest analyzed allelic variability. Thus, the number of QTLs detected per variable varied from three for NbDetA to seven for AngLA2, all populations taken together. All LGs were involved, yet with a strong implication of LG2. Most QTLs located on this LG had a major effect and were stable. We detected five new QTLs, located on LGs 2, 6, and 7, for the branching angle of axes, and the QTL located on LG7 co-localized with *RhBRC1*, a branching repressor (Barbier et al. 2015; Rameau et al. 2015). Other QTLs, involved in the control of branching and stem elongation, also co-localized with *RhBRC1*, highlighting its pleiotropic nature.

We also revealed year-specific QTLs that genetically explained the $G \times Y$ interactions observed for NbSA3 and AngLA2. Finally, the use of connected populations for the genetic analysis of these variables highlighted for the first time the effect of the genetic background on the detection of QTLs in rose bush.

The QTL analysis could be extended to a greater number of connected populations (i.e., multiparental approach)—already available (Crespel et al. 2002; Kawamura et al. 2011). In addition to broadening the allelic variability, it would help to increase QTL detection power, the accuracy of QTL locations, and the robustness of estimation of QTLs effects, but also to evaluate the QTL effects in different genetic backgrounds, as it was recently shown in apple tree (Bink et al. 2014; Allard et al. 2016).

The present study on the heritability and heredity of rose bush architecture provides new insights into the topic that will obviously be of great help to better design and lead the genetic improvement programs for plant architecture and, in turn, rose bush shape.

Acknowledgements The authors would like to thank Rémi Gardet and his team of the IRHS experimental station (ImHorPhen) for their technical assistance in plant management, Muriel Bahut of the ANAN platform (SFR QuaSaV) and Charles Poncet of the Gentyane platform for SSR analyses, Hervé Autret and Marie-Sophie Neveux for their technical assistance, Valérie Le Clerc for proofreading this manuscript in depth, and Annie Buchwalter for proofreading the English language in this manuscript.

Funding information This study was financed by the French Ministry of Agriculture and Fisheries (Compte d'Affectation Spéciale pour le Développement Agricole et Rural; CASDAR) within the framework of the ARIAGE project.

Compliance with ethical standards

Conflict of interest The authors declare that they have no conflict of interest.

Data archiving statement All relevant data are within the article and supplementary material files.

References

Aguilar-Martinez JA, Poza-Carrion C, Cubas P (2007) *Arabidopsis* BRANCHED1 acts as an integrator of branching signals within axillary buds. Plant Cell 19:458–472. https://doi.org/10.1105/tpc.106.048934

Allard A, Bink MCAM, Martinez S, Kelner JJ, Legave JM, di Guardo M, Di Pierro EA, Laurens F, van de Weg EW, Costes E (2016) Detecting QTLs and putative candidate genes involved in budbreak and flowering time in an apple multiparental population. J Exp Bot 67:2875–2888. https://doi.org/10.1093/jxb/erw130

Alméras T, Costes E, Salles JC (2004) Identification of biomechanical factors involved in stem shape variability between apricot tree varieties. Ann Bot 93:455–468. https://doi.org/10.1093/aob/mch054

Banerjee S, Yandell BS, Yi N (2008) Bayesian quantitative trait loci mapping for multiple traits. Genetics 179:2275–2289. https://doi.org/10.1534/genetics.108.088427

Barbier F, Péron T, Lecerf M, Perez-Garcia MD, Barrière Q, Rolík J, Boutet-Mercy S, Citerne S, Lemoine R, Porcheron B, Roman H, Leduc N, Le Gourriérec J, Bertheloot J, Sakr S (2015) Sucrose modulates the key hormonal mechanisms controlling bud outgrowth in *Rosa hybrida*. J Exp Bot 66:2569–2582. https://doi.org/10.1093/jxb/erv047

Beavis WD, Grant D, Albertsen M, Fincher R (1991) Quantitative trait loci for plant height in four maize populations and their associations with qualitative genetic loci. Theor Appl Genet 83:141–145

Ben Sadok I, Celton JM, Essalouh L, El Aabidine AZ, Garcia G, Martinez S, Grati-Kamoun N, Rebai A, Costes E, Khadari B (2013) QTL mapping of flowering and fruiting traits in olive. PLoS One 8:e62831. https://doi.org/10.1371/journal.pone.0062831

Billotte N, Jourjon MF, Marseillac N, Berger A, Flori A, Asmady H, Adon B, Singh R, Nouy B, Potier F, Cheah SC, Rohde W, Ritter E, Courtois B, Charrier A, Mangin B (2010) QTL detection by multi-parent linkage mapping in oil palm (*Elaeis guineensis* Jacq.) Theor Appl Genet 120:1673–1687. https://doi.org/10.1007/s00122-010-1284-y

Bink MCAM, Jansen J, Madduri M, Voorrips RE, Durel CE, Kouassi AB, Laurens F, Mathis F, Gessler C, Gobbin D, Rezzonico F, Patocchi A, Kellerhals M,·Boudichevskaia A, Dunemann F, Peil A, Nowicka A, Lata B, Stankiewicz-Kosy M, Jeziorek K, Pitera E, Soska A, Tomala K, Evans KM, Fernández-Fernández F, Guerra W, Korbin M, Keller S, Lewandowski M, Plocharski W, Rutkowski K, Zurawicz E, Costa F, Sansavini S, Tartarini S, Komjanc M, Mott D, Antofie A, Lateur M, Rondia A, Gianfranceschi L, van de Weg WE (2014). Bayesian QTL analyses using pedigreed families of an outcrossing species, with application to fruit firmness in apple. Theor Appl Genet 127, 1073–1090. doi:https://doi.org/10.1007/s00122-014-2281-3

Blanc G, Charcosset A, Mangin B, Gallais A, Moreau L (2006) Connected populations for detecting quantitative trait loci and

testing for epistasis: an application in maize. Theor Appl Genet 113: 206–224. https://doi.org/10.1007/s00122-006-0287-1

Boumaza R, Demotes-Mainard S, Huche-Thelier L, Guerin V (2009) Visual characterization of the esthetic quality of the rosebush. J Sens Stud 24:774–796. https://doi.org/10.1111/j.1745-459X.2009.00238.x

Bredmose NB (1998) Growth flowering and postharvest performance of single stemmed rose (*Rosa hybrida* L.) in response to light quantum integral and plant population density. J Amer Soc Hort Sci 123:569–576

Celton JM, Martinez S, Jammes MJ, Bechti A, Salvi S, Legave JM, Costes E (2011) Deciphering the genetic determinism of bud phenology in apple progenies: a new insight into chilling and heat requirement effects on flowering dates and positional candidate genes. New Phytol 192:378–392. https://doi.org/10.1111/j.1469-8137.2011.03823.x

Crespel L, Chirollet M, Durel CE, Zhang D, Meynet J, Gudin S (2002) Mapping of qualitative and quantitative phenotypic traits in Rosa using AFLP markers. Theor Appl Genet 105:1207–1214

Crespel L, Sigogne M, Donès N, Relion D, Morel P (2013) Identification of relevant morphological, topological and geometrical variables to characterize the architecture of rose bushes in relation to plant shape. Euphytica 191:129–140. https://doi.org/10.1007/s10681-013-0902-6

Crespel L, Le Bras C, Relion D, Morel P (2014) Genotype × year interaction and broad-sense heritability of architectural characteristics in rose bush. Plant Breed 133:412–418. https://doi.org/10.1111/pbr.12157

Dai B, Guo H, Huang C, Ahmed MM, Lin Z (2017) Identification and characterization of segregation distortion loci on cotton chromosome 18. Front Plant Sci 7:2037. https://doi.org/10.3389/fpls.2016.02037

De Vienne D, Causse M (1998) La cartographie et la caractérisation des locus contrôlant la variation des caractères quantitatifs. In de Vienne (ed) Les marqueurs moléculaires en génétique et biotechnologies végétales, 2nd edn. INRA, pp 89–118

Debener T, Linde M (2009) Exploring complex ornamental genomes: the rose as a model plant. Crit Rev Plant Sci 28:267–280. https://doi.org/10.1080/07352680903035481

Debener T, Bretzke M, Spiller M, Linde M, Kaufmann H, Berger RG, Krings U (2010) Genetic and molecular analyses of key loci involved in self-incompatibility and floral scent in roses. Acta Hortic 870:183–190

Demotes-Mainard S, Huché-Thélier L, Morel P, Boumaza R, Guérin V, Sakr S (2013) Temporary water restriction or light intensity limitation promotes branching in rose bush. Sci Hortic 150:432–440. https://doi.org/10.1016/j.scienta.2012.12.005

Demotes-Mainard S, Péron T, Corot A, Bertheloot J, Le Gourrierec J, Pelleschi-Travier S, Crespel L, Morel P, Huché-Thélier L, Boumaza R, Vian A, Guérin V, Leduc N, Sakr S (2016) Plant responses to red and far-red lights, applications in horticulture. Environ Exp Bot 121: 4–21. https://doi.org/10.1016/j.envexpbot.2015.05.010

Djennane S, Hibrand-Saint Oyant L, Kawamura K, Lalanne D, Laffaire M, Thouroude T, Chalain S, Sakr S, Boumaza R, Foucher F, Leduc N (2013) Impacts of light and temperature on shoot branching gradient and expression of strigolactone synthesis and signalling genes in rose. Plant Cell Environ 37:742–757. https://doi.org/10.1111/pce.12191

Donès N, Adam B, Sinoquet H (2006) PiafDigit software. http://www1.clermont.inra.fr/piaf/fr/telechargement/telecharger.php. Accessed 25 Apr 2017

Finlayson SA, Krishnareddy SR, Kebrom TH, Casal JJ (2010) Phytochrome regulation of branching in *Arabidopsis*. Plant Physiol 152:1914–1927. https://doi.org/10.1104/pp.109.148833

Girault T, Bergougnoux V, Combes D, Viemont JD, Leduc N (2008) Light controls shoot meristem organogenic activity and leaf primordia growth during bud burst in *Rosa* sp. Plant Cell Environ 31:1534–1544. https://doi.org/10.1111/j.1365-3040.2008.01856.x

Gitonga VW, Koning-Boucoiran CFS, Verlinden K, Dolstra O, Visser RGF, Maliepaard C, Krens FA (2014) Genetic variation, heritability and genotype by environment interaction of morphological traits in a tetraploid rose population. BMC Genet 15:146. https://doi.org/10.1186/s12863-014-0146-z

Godin C, Caraglio Y (1998) A multiscale model of plant topological structures. J Theor Biol 191:1–46

Godin C, Costes E, Sinoquet H (1999) A method for describing plant architecture which integrates topology and geometry. Ann Bot 84: 343–357. https://doi.org/10.1006/anbo.1999.0923

Gomez-Roldan V, Fermas S, Brewer PB, Puech-Pagès V, Dun EA, Pillot JP, Letisse F, Matusova R, Danoun S, Portais JC, Bouwmeester H, Bécard G, Beveridge CA, Rameau C, Rochange SF (2008) Strigolactone inhibition of shoot branching. Nature 455:189–194. https://doi.org/10.1038/nature07271

Gudin S (2000) Rose: genetics and breeding. Plant Breed Rev 17:159–189

Henry C, Rabot A, Laloi M, Mortreau E, Sigogne M, Leduc N, Lemoine R, Sakr S, Vian A, Pelleschi-Travier S (2011) Regulation of *RhSUC2*, a sucrose transporter, is correlated with the light control of bud burst in *Rosa* sp. Plant Cell Environ 34:1776–1789. https://doi.org/10.1111/j.1365-3040.2011.02374.x

Hibrand-Saint Oyant L, Crespel L, Rajapakse S, Zhang L, Foucher F (2008) Genetic linkage maps of rose constructed with new microsatellite markers and locating QTL controlling flowering traits. Tree Genet Genomes 4:11–23. https://doi.org/10.1007/s11295-007-0084-2

Huang YF, Doligez A, Fournier-Level A, Le Cunff L, Bertrand Y, Canaguier A, Morel C, Miralles V, Veran F, Souquet JM, Cheynier V, Terrier N, This P (2012) Dissecting genetic architecture of grape proanthocyanidin composition through quantitative trait locus mapping. BMC Plant Biol 12:30. https://doi.org/10.1186/1471-2229-12-30

Huché-Thélier L, Boumaza R, Demotes-Mainard S, Canet A, Symoneaux R, Douillet O, Guérin V (2011) Nitrogen deficiency increases basal branching and modifies visual quality of the rose bushes. Sci Hortic 130:325–334. https://doi.org/10.1016/j.scienta.2011.07.007

Huché-Thélier L, Crespel L, Le Gourrierec J, Morel P, Sakr S, Leduc N (2016) Light signaling and plant responses to blue and UV radiations—perspectives for applications in horticulture. Environ Exp Bot 121:22–38. https://doi.org/10.1016/j.envexpbot.2015.06.009

Iwata H, Gaston A, Remay A, Thouroude T, Jeauffre J, Kawamura K, Hibrand Saint-Oyant L, Araki T, Denoyes B, Foucher F (2012) The TFL1 homologue KSN is a regulator of continuous flowering in rose and strawberry. Plant J 69:116–125. https://doi.org/10.1111/j.1365-313X.2011.04776.x

Kawamura K, Hibrant-Saint Oyant L, Crespel L, Thouroude T, Lalanne D, Foucher F (2011) Quantitative trait loci for flowering time and inflorescence architecture in rose. Theor Appl Genet 122:661–675. https://doi.org/10.1007/s00122-010-1476-5

Kawamura K, Hibrand-Saint Oyant L, Thouroude T, Jeauffre J, Foucher F (2015) Inheritance of garden rose architecture and its association with flowering behaviour. Tree Genet Genomes 11:1–12. https://doi.org/10.1007/s11295-015-0844-3

Klie M, Menz I, Linde M, Debener T (2015) Strigolactone pathway genes and plant architecture: association analysis and QTL detection for horticultural traits in chrysanthemum. Mol Gen Genomics 291:957–969. https://doi.org/10.1007/s00438-015-1155-y

Knapp SJ, Bridges WC (1990) Using molecular markers to estimate quantitative trait locus parameters: power and genetic variances for unreplicated and replicated progeny. Genetics 126:769–777

Leduc N, Roman H, Barbier F, Péron T, Huché-Thélier L, Lothier J, Demotes-Mainard S, Sakr S (2014) Light signaling in bud outgrowth and branching inplants. Plants 3:223–250

Li YL, Niu SZ, Dong YB, Cui DQ, Wang YZ, Liu YY, Wei MG (2007) Identification of trait-improving quantitative trait loci for grain yield components from a dent corn inbred line in an advanced backcross BC_2F_2 population and comparison with its $F_{2:3}$ population in popcorn. Theor Appl Genet 115:129–140. https://doi.org/10.1007/s00122-007-0549-6

Li YL, Li XH, Li JZ, Fu JF, Wang YZ, Wei MG (2009) Dent corn genetic background influences QTL detection for grain yield and yield components in high-oil maize. Euphytica 169:273–284. https://doi.org/10.1007/s10681-009-9966-8

Li-Marchetti C, Le Bras C, Relion D, Citerne S, Huché-Thélier L, Sakr S, Morel P, Crespel L (2015) Genotypic differences in architectural and physiological responses to water restriction in rose bush. Front Plant Sci 6:355. https://doi.org/10.3389/fpls.2015.00355

Lorieux M, Goffinet B, Perrier X, Gonzalez de Leon D, Lanaud C (1995a) Maximum likelihood models for mapping genetic markers showing segregation distortion. 1. Backcross population. Theor Appl Genet 90:73–80

Lorieux M, Perrier X, Goffinet B, Lanaud C, Gonzalez de Leon D (1995b) Maximum likelihood models for mapping genetic markers showing segregation distortion. 2. F2 population. Theor Appl Genet 90:81–89

Meng J, Li D, Yi T, Yang J, Zhao X (2009) Development and characterization of microsatellite loci for *Rosa odorata* var. *gigantea* Rehder & E. H. Wilson (*Rosaceae*). Conserv Genet 10:1973–1976. https://doi.org/10.1007/s10592-009-9871-7

Meyer JDF, Snook MEK, Houchins E, Rector BG, Widstrom NW, McMullen MD (2007) Quantitative trait loci for maysin synthesis in maize (*Zea mays* L.) lines selected for high silk maysin content. Theor Appl Genet 115:119–128. https://doi.org/10.1007/s00122-007-0548-7

Moghaddam HH, Leus L, De Riek J, Van Huylenbroeck J, Van Bockstaele E (2012) Construction of a genetic linkage map with SSR, AFLP and morphological markers to locate QTLs controlling pathotype-specific powdery mildew resistance in diploid roses. Euphytica 184:413–427. https://doi.org/10.1007/s10681-011-0616-6

Morel P, Galopin G, Donès N (2009) Using architectural analysis to compare the shape of two hybrid tea rose genotypes. Sci Hortic 120:391–398. https://doi.org/10.1016/j.scienta.2008.11.039

Morel P, Crespel L, Galopin G, Moulia B (2012) Effect of mechanical stimulation on the growth and branching of garden rose. Sci Hortic 135:59–64. https://doi.org/10.1016/j.scienta.2011.12.007

Nanson A (1970) L'héritabilité et le gain d'origine génétique dans quelques types d'expériences. Silvae Genet 19:113–121

Niwa M, Daimon Y, Kurotani K, Higo A, Pruneda-Paz JL, Breton G, Mitsuda N, Kay SA, Ohme-Takagi M, Endo M, Arakia T (2013) BRANCHED1 interacts with FLOWERING LOCUS T to repress the floral transition of the axillary meristems in *Arabidopsis*. Plant Cell 25:1228–1242. https://doi.org/10.1105/tpc.112.109090

Pauly L, Flajoulot S, Garon J, Julier B, Béguier V, Barre P (2012) Detection of favorable alleles for plant height and crown rust tolerance in three connected populations of perennial ryegrass (*Lolium perenne* L.) Theor Appl Genet 124:1139–1153. https://doi.org/10.1007/s00122-011-1775-5

Rameau C, Bertheloot J, Leduc N, Andrieu B, Foucher F, Sakr S (2015) Multiple pathways regulate shoot branching. Front Plant Sci 5:741. https://doi.org/10.3389/fpls.2014.00741

Roman H, Rapicault M, Miclot AS, Larenaudie M, Kawamura K, Thouroude T, Chastellier A, Lemarquand A, Dupuis F, Foucher F, Loustau S, Hibrand-Saint Oyant L (2015) Genetic analysis of the flowering date and number of petals in rose. Tree Genet Genomes 11:85. https://doi.org/10.1007/s11295-015-0906-6

Segura V, Cilas C, Laurens F, Costes E (2006) Phenotyping progenies for complex architectural traits: a strategy for 1-year-old apple trees (*Malus* x *domestica* Borkh.) Tree Genet Genomes 2:140–151. https://doi.org/10.1007/s11295-006-0037-1

Segura V, Denancé C, Durel CE, Costes E (2007) Wide range QTL analysis for complex architectural traits in 1-year-old apple progeny. Genome 50:159–171. https://doi.org/10.1139/G07-002

Shin HK, Lieth JH, Kim SH (2001) Effects of temperature on leaf area and flower size in rose. Acta Hortic 547:185–191

Souza VAB, Byrne DH, Taylor JF (1998) Heritability, genetic and phenotypic correlations, and predicted selection response of quantitative traits in peach: II. An analysis of several fruit traits. J Am Soc Hortic Sci 123:604–611

Spiller M, Linde M, Hibrand-Saint Oyant L, Tsai CJ, Byrne DH, Smulders MJM, Foucher F, Debener T (2011) Towards a unified genetic map for diploid roses. Theor Appl Genet 122:489–500. https://doi.org/10.1007/s00122-010-1463-x

Teichmann T, Muhr M (2015) Shaping plant architecture. Front Plant Sci 6:233. https://doi.org/10.3389/fpls.2015.00233

Umehara M, Hanada A, Yoshida S, Akiyama K, Arite T, Takeda-Kamiya N, Magome H, Kamiya Y, Shirasu K, Yoneyama K, Kyozuka J, Yamaguchi S (2008) Inhibition of shoot branching by new terpenoid plant hormones. Nature 455:195–200. https://doi.org/10.1038/nature07272

Van Ooijen JW (2011) Multipoint maximum likelihood mapping in a full-sib family of an outbreeding species. Genet Res 93:343–349. https://doi.org/10.1017/S0016672311000279

Voorrips RE (2002) MapChart: software for the graphical presentation of linkage maps and QTLs. J Hered 93:77–78

White J (1979) The plant as a metapopulation. Annu Rev Ecol Syst 10:109–145. https://doi.org/10.1146/annurev.es.10.110179.000545

Yan Z, Denneboom C, Hattendorf A, Dolstra O, Debener T, Stam P, Visser PB (2005) Construction of an integrated map of rose with AFLP, SSR, PK, RGA, RFLP, SCAR and morphological markers. Theor Appl Genet 110:766–777. https://doi.org/10.1007/s00122-004-1903-6

Yan Z, Visser PB, Hendriks T, Prins TW, Stam P, Dolstra O (2007) QTL analysis of variation for vigour in rose. Euphytica 154:53–62. https://doi.org/10.1007/s10681-006-9269-2

Zhang L, Wang S, Li H, Deng Q, Zheng A, Li S, Li P, Li Z, Wang J (2010) Effects of missing marker and segregation distortion on QTL mapping in F_2 populations. Theor Appl Genet 121:1071–1082. https://doi.org/10.1007/s00122-010-1372-z

Zieslin N, Mor Y (1990) Light on roses. A review. Scientia Hort 43:1–14